The Meteoritical Society

Meteoritics & Planetary Science 50, Nr 6, 1089–1111 (2015)
doi: 10.1111/maps.12456

The Vicência meteorite fall: A new unshocked (S1) weakly metamorphosed (3.2) LL chondrite

Klaus KEIL[1*], Maria E. ZUCOLOTTO[2], Alexander N. KROT[1], Patricia M. DOYLE[1], Myriam TELUS[1], Tatiana V. KROT[1], Richard C. GREENWOOD[3], Ian A. FRANCHI[3], John T. WASSON[4], Kees C. WELTEN[5], Marc W. CAFFEE[6], Derek W. G. SEARS[7], My RIEBE[8], Rainer WIELER[8], Edivaldo dos SANTOS[9], Rosa B. SCORZELLI[9], Jerome GATTACCECA[10], France LAGROIX[11], Matthias LAUBENSTEIN[12], Julio C. MENDES[13], Philippe SCHMITT-KOPPLIN[14], Mourad HARIR[14], and Andre L. R. MOUTINHO[15]

[1]Hawaii Institute of Geophysics and Planetology, School of Ocean and Earth Science and Technology, University of Hawaii at Mānoa, Honolulu, Hawaii 96822, USA
[2]Museu Nacional/UFRJ, Quinta da Boa Vista—RJ, Rio de Janeiro CEP 20.940-040, Brazil
[3]Planetary and Space Sciences, The Open University, Walton Hall, Milton Keynes MK7 6AA, UK
[4]Departments of Earth and Space Sciences and Chemistry and Biochemistry, Institute of Geophysics and Planetary Physics, University of California, Los Angeles, California 90095–1567, USA
[5]Space Sciences Laboratory, University of California, Berkeley, California 94720–7450, USA
[6]Department of Physics, Purdue University, West Lafayette, Indiana 47907–2036, USA
[7]Space Science and Astrobiology Division, NASA Ames Research Center, MS 245-3, Moffett Field, Mountain View, California 94035, USA
[8]Department of Earth Sciences, ETH Zürich, NW C 82, Zürich CH-8092, Switzerland
[9]Centro Brasileiro de Pesquisas Físicas, Rua Dr. Xavier Sigaud 150, Rio de Janeiro 22290-180, Brazil
[10]CEREGE UM 34, CNRS/Aix-Marseille University, Aix-en-Provence 13545, France
[11]IPGP, Paris, France
[12]Laboratori Nazionali del Gran Sasso, Istituto Nazionale di Fisica Nucleare, Via G. Acitelli 22, Assergi (AQ) I-67100, Italy
[13]Departamento de Geologia, UFRJ, Av. Athos da Silveira Ramos, 274. Cidade Universitária, Rio de Janeiro, Brazil
[14]Department of Environmental Sciences (DES), Helmholtz Zentrum München, Ingolstädter Landstrasse 1, Neuherberg 85764, Germany
[15]R. Francisco Ricci, 181 33D Vila Ema, São José dos Campos/SP, São Paulo CEP 12.243-261, Brazil
[*]Corresponding author: E-mail: keil@hawaii.edu

(Received 10 November 2014; revision accepted 17 March 2015)

Abstract–The Vicência meteorite, a stone of 1.547 kg, fell on September 21, 2013, at the village Borracha, near the city of Vicência, Pernambuco, Brazil. It was recovered immediately after the fall, and our consortium study showed it to be an unshocked (S1) LL3.2 ordinary chondrite. The LL group classification is based on the bulk density (3.13 g cm^{-3}); the chondrule mean apparent diameter (0.9 mm); the bulk oxygen isotopic composition ($\delta^{17}O = 3.768 \pm 0.042‰$, $\delta^{18}O = 5.359 \pm 0.042‰$, $\Delta^{17}O = 0.981 \pm 0.020‰$); the content of metallic Fe,Ni (1.8 vol%); the Co content of kamacite (1.73 wt%); the bulk contents of the siderophile elements Ir and Co versus Au; and the ratios of metallic Fe^0/total iron (0.105) versus total Fe/Mg (1.164), and of Ni/Mg (0.057) versus total Fe/Mg. The petrologic type 3.2 classification is indicated by the beautifully developed chondritic texture, the standard deviation (~0.09) versus mean Cr_2O_3 content (~0.14 wt%) of ferroan olivine, the TL sensitivity and the peak temperature and peak width at half maximum, the cathodoluminescence properties of chondrules, the content of trapped $^{132}Xe_{tr}$ (0.317×10^{-8} cm^3STP g^{-1}), and the Raman spectra for organic material in the matrix. The cosmic ray exposure age is ~72 Ma, which is at the upper end of the age distribution of LL group chondrites. The meteorite is unusual in that it contains relatively large, up to nearly 100 μm in size, secondary fayalite grains, defined as olivine with $Fa_{>75}$, large enough to allow

in situ measurement of oxygen and Mn-Cr isotope systematics with SIMS. Its oxygen isotopes plot along a mass-dependent fractionation line with a slope of ~0.5 and $\Delta^{17}O$ of 4.0 ± 0.3‰, and are similar to those of secondary fayalite and magnetite in the unequilibrated chondrites EET 90161, MET 96503, and Ngawi. These data suggest that secondary fayalite in Vicência was in equilibrium with a fluid with a $\Delta^{17}O$ of ~4‰, consistent with the composition of the fluid in equilibrium with secondary magnetite and fayalite in other unequilibrated ordinary chondrites. Secondary fayalite and the chondrule olivine phenocrysts in Vicência are not in isotopic equilibrium, consistent with low-temperature formation of fayalite during aqueous alteration on the LL parent body. That alteration, as dated by the ^{53}Mn-^{53}Cr chronology age of secondary fayalite, took place $4.0^{+1.4}_{-1.1}$ Ma after formation of CV CAIs when anchored to the quenched angrite D'Orbigny.

INTRODUCTION

The Vicência meteorite, a single stone weighing 1.547 kg and measuring 13.7 × 12 × 8.5 cm (Fig. S1), fell on September 21, 2013, at about 15:00 h local time (18:00 UTC), at the village Borracha (Figs. S2a and S2b) near the small city of Vicência, about 120 km from the capital of Recife, State of Pernambuco, Brazil (Moutinho and Zucolotto 2014). It landed less than 1 m from Mr. Adeildo Silva (Figs. S3a and S3b), who was fixing a wood wagon on a sunny day outside his joinery. He suddenly heard a very loud noise of something that had just hit the ground near him, but no sound in the air or a bolide had been noticed by him and other residents in the area. He did not know what had happened, but soon noticed a very strange black rock in a small pit and claims that one side of the rock was warm, whereas the other was cold. Notice of the event in the media on September 27, 2013 prompted two of us (MEZ, AM) to visit Borracha on September 28, 2013 and purchase the meteorite on September 30, 2013 from the finder (Fig. S4). We also searched on the nearby mountains for possible additional pieces of the fall. However, the area is covered by dense vegetation of banana plantations (Fig. S2b), not favorable for the recovery of additional stones, and no additional material was found by us nor delivered to us by other residents of the area, who we had contacted. Four polished thin sections are deposited in the Museu Nacional, Rio de Janeiro.

Analytical Techniques

In Data S1, the details of the analytical techniques used in this study are described.

RESULTS

Macroscopic Description, Density, and Porosity

The meteorite is covered nearly entirely by a dull to shiny, ~3 mm thick, black fusion crust (Fig. S1). A rough secondary crust on one side of the stone suggests that it broke up late during entry into the atmosphere. On cut surfaces, the pronounced chondritic texture is clearly visible, with abundant and beautifully developed chondrules up to ~7 mm in diameter and numerous what appear to be chondrule, mineral, and rock fragments up to ~7 mm in diameter (Figs. 1 and S5). Chondrules and fragments are embedded into a gray to black, fine-grained matrix.

The volume of the entire stone was determined in a 3-D scanner to be 495.826 cm^3. The bulk density of 3.13 g cm^{-3} was calculated from the volume and mass of the stone. The grain density determined using a Jolly balance of a small piece is 3.28 g cm^{-3}, suggesting a porosity of 4.75%.

Mineralogy and Petrology

The Vicência meteorite is unshocked (shock stage S1 of Stöffler et al. 1991) and has the typical well-developed chondritic texture, mineralogy, and mineral compositions of a highly unequilibrated ordinary chondrite (UOC). The measured apparent chondrule diameters range from ~0.2 to 2.8 mm. Excluding some of the few very large chondrules, we consider 0.9 mm as a reasonable estimate of their mean diameter. Modal analyses of three polished thin sections yield the following volume percent abundances: 65 chondrules, 12 dark matrix, 6 metallic FeNi + troilite, the remainder being made up of chondrule fragments and unidentified grains. The chondritic texture is pronounced, with abundant type I and type II and beautifully developed porphyritic olivine and radial pyroxene chondrules dominating the texture (Figs. S6 and 1–4). Some chondrules contain relict "dusty" olivine (Figs. 3a and 3b). Relict forsteritic olivine also occurs in type II chondrules (Fig. 3c). Several chondrules are aluminum-rich (Figs. 2f and 4); one of these chondrules (Figs. 4a–d) contains very sodium-rich glassy mesostasis surrounding coarse euhedral and skeletal crystals of

Fig. 1. Cut surface of the Vicência chondrite, showing abundant and beautifully developed chondrules and what appear to be chondrule, mineral and rock fragments, embedded into a gray to black, fine-grained matrix.

spinel, forsteritic olivine, and aluminum-diopside. Some of the chondrules have been altered by parent body processes, resulting, for example, in the formation of secondary fayalite (Fig. 3d).

The major constituent minerals are olivine and low-Ca pyroxene of highly variable composition of ~$Fa_{0–45}$ and ~$Fs_{0–30}$ (Fig. 5). In addition shown are the MnO and Cr_2O_3 contents of chondrule olivine, with a mean Cr_2O_3 content in olivine of ~0.14 wt% and a standard deviation of ~0.09.

The meteorite is unusual in that it contains relatively large, up to nearly 100 μm in size, secondary fayalite in the matrix, defined as olivine with $Fa_{>75}$ (in Fig. 5, referred to as matrix olivine). It occurs as coarse grains between the chondrules, as overgrowths of chondrule olivine fragments (Figs. 6b–f), and as small grains in fine-grained rims (Fig. 6a). In some cases, ferroan olivine replaces opaque nodules and low-Ca pyroxene in type I chondrule peripheries (Fig. 6a). Some fayalite grains show inverse compositional zoning (Figs. 6e and 6f), indicating postcrystallization Fe-Mg diffusion. The secondary fayalite grains are large enough to allow in situ measurements of oxygen and Mn-Cr systematics with the SIMS (see below).

Twenty-five chondrules were located in cathodoluminescence images and assigned to chemical classes A1–A5 and B1–B3 (DeHart et al. 1992; Sears et al. 1992). Two chondrules are class A1, nine are A2, three are A5, seven are B1, three are B2, and one could not be classified. The distribution of these chondrules over the classes is shown in Fig. 7, where they are compared to similar data for nine other ordinary chondrites (Sears et al. 1995).

The content of metallic Fe, Ni was estimated by image processing of Ni Kα X-ray maps (Fig. 2d) with the ImageJ program and was found to vary between 1 and 2.4 vol% (average 1.8 vol%). This and the visual inspection of polished thin sections in reflected light (e.g., Fig. S6c) indicate that the content of metallic Fe, Ni is relatively low. Similar values are also indicated by the magnetic hysteresis properties which point to a metal content of about 3.5 wt% (1.4 vol%), mostly in the form of kamacite. These contents were also confirmed by Mössbauer analysis and are close to the mean of LL group ordinary chondrites (Krot et al. 2014). In addition, the compositions of kamacite (5.86 ± 0.8 wt% Ni, 1.73 ± 0.3 wt% Co), and of zoned taenite (36.2 ± 2.7 wt % Ni) were measured with an electron probe micro analyzer (EPMA). Finally, the metallographic cooling rates of taenite grains were determined and found to range between ~50 and 60 K Ma^{-1} (Fig. S7).

Raman spectra of organic material from the matrix of chondrites are useful for constraining the metamorphic grade of chondrites. The first-order carbon spectra consist of D- (~1350 cm^{-1}) and G-bands (~1600 cm^{-1}) from disordered carbon and graphite, respectively. These bands are sensitive to thermal metamorphism (Fig. S8). Quirico et al. (2003) and Bonal et al. (2006, 2007) found that the width of the D-band (FWHM-D) and the ratio of the intensity of the D- and G-peaks (I_D/I_G) correlate with the metamorphic grade of chondrites. The main assumption of these studies is that the carbonaceous material in the matrix of different chondrites share the same precursor and heating conditions.

Our analyses of QUE 97008 and GRO 95544 are consistent with previous results for these chondrites (Fig. S8). The data for Vicência (Fig. 8) are consistent within the uncertainties of it being of petrologic type 3.2. QUE97008 and GRO95544 are Antarctic finds, and comparison of Vicência to other ordinary chondrite falls like Semarkona and Krymka indicates that the data for Vicência are more consistent with Tieschitz, an H/L type 3.6 chondrite fall. These results indicate that the organic materials in the Vicência matrix have experienced peak temperatures between 400 and 600 °C, typical of type 3.2–3.6 chondrites (Huss et al. 2006).

The Mössbauer spectrum of the bulk sample (Fig. 9a) arises from the overlapping of two quadrupole doublets attributed to olivine and pyroxene, both paramagnetic silicates, and two magnetic sextets attributed to troilite and kamacite. Due to the high amount of troilite and silicates, it is difficult to detect the L_{10} superstructure phase tetrataenite in the meteorite bulk sample. However, the spectrum of separated metal particles (Fig. 9b), in spite of the presence of a small amount of olivine, exhibits kamacite and taenite. Antitaenite, intergrown with tetrataenite, is also visible (Rancourt and Scorzelli 1995). Hyperfine parameters are shown in Table 1.

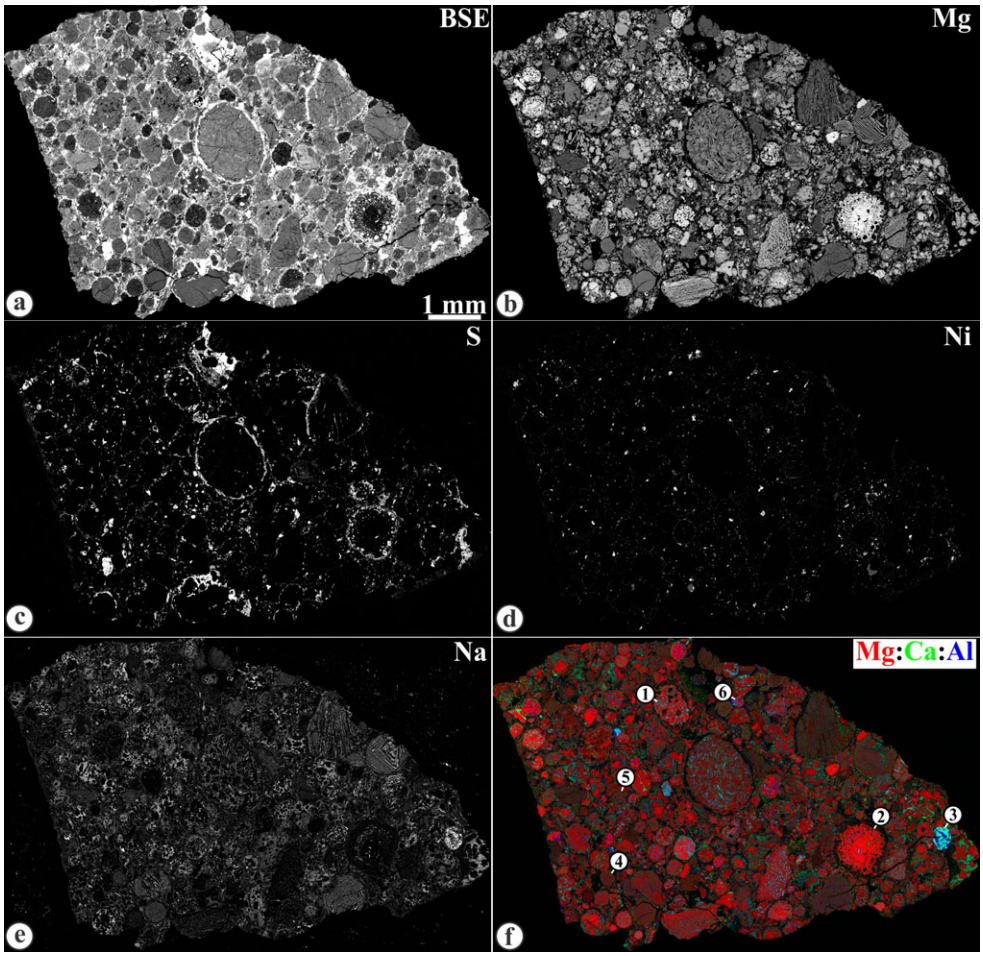

Fig. 2. a) Backscattered electron image of a polished thin section of Vicência, b–e) elemental maps of the same section in (b) Mg, (c) S, (d) Ni, and (e) Na Kα X-rays, and (f) combined elemental map in Mg (red), Ca (green), and Al Kα (blue) X-rays. Numbered objects in (f) are referred to in Figs. 3 and 4 and in the text.

Bulk Composition

Bulk Composition Measured by ICP-OES

The bulk composition of a small aliquot of the dissolved sample of a 101.4 mg chip from the analysis of long-lived radionuclides was measured by ICP-OES for 11 elements, including, Fe, Ni, and Co. Their contents are close to average LL group chondrites (Table 2).

Major, Minor, and Trace Elements Measured by Instrumental Neutron Activation Analysis (INAA)

Our data for 24 elements are summarized in Table 3. Abundances of refractory lithophile elements are roughly constant in each chondrite group, and closely similar in the three groups of ordinary chondrites (Fig. S9). Refractory lithophile element abundances in ordinary chondrites are about 90% of those in CI chondrites (Wasson and Kallemeyn 1988). In Fig. S9, H-chondrite and Cr-normalized abundance ratios for Vicência and, for comparison, for CI, L, and LL chondrites (Wasson and Kallemeyn 1988; Kallemeyn et al. 1989) are shown. The L and LL chondrites plot very close to unity, and the CI chondrites somewhat above. Vicência also plots close to unity, confirming the petrographic and isotopic data indicating it is an ordinary chondrite. Some changes (up to 4%) have been made in the older data to allow for differences resulting from a change in our elemental standards.

The three siderophile elements that we determine with the best precision are Co, Ir, and Au; in Fig. 10 we plot Ir and Co versus Au, together with the data for L and LL chondrites of Kallemeyn et al. (1989). The two sets of data are well resolved in terms of all three elements. Vicência plots near the high-siderophile element end of the cloud of LL points (we have not corrected for the fact that our new Au data are systematically about 4% higher than those of Kallemeyn et al. 1989).

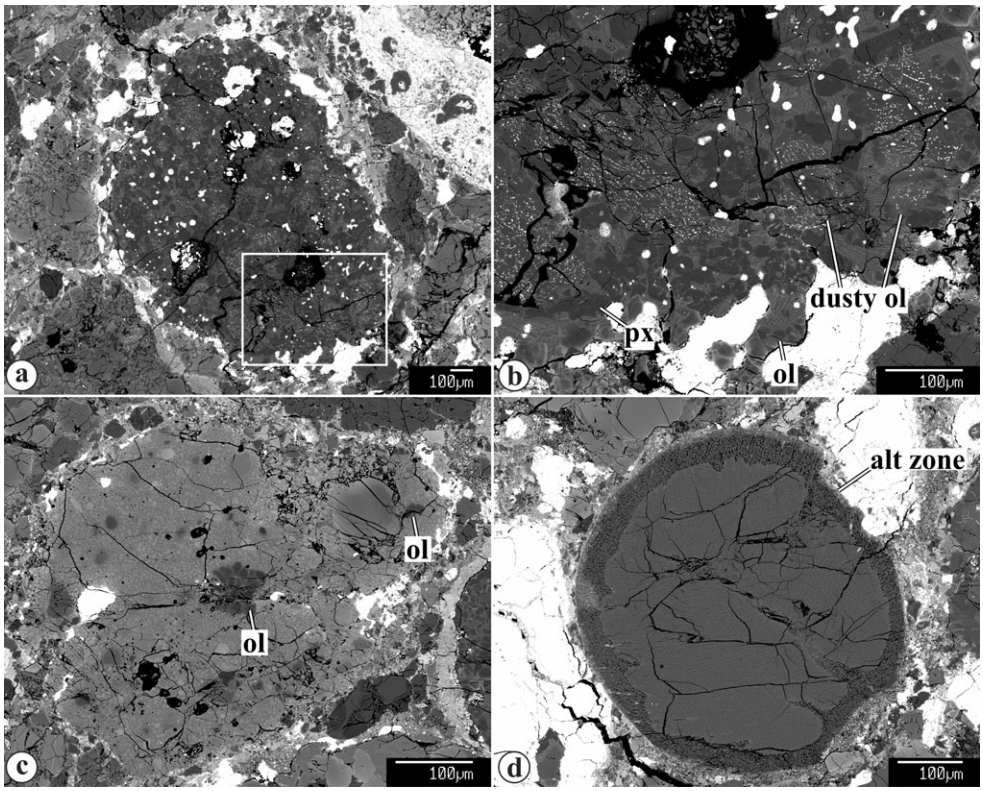

Fig. 3. Backscattered electron images of chondrules from Vicência. a, b) Type I chondrule (labeled as 1 in Fig. 2f) with abundant relict dusty olivine grains. Region outlined in (a) is shown in detail in (b). c) Type II chondrule containing relict forsteritic olivines. d) Bleached cryptocrystalline chondrule (labeled as 4 in Fig. 2f).

Oxygen Isotopic Composition

Oxygen isotopic analyses are reported in standard δ notation, where $\delta^{18}O$ has been calculated as: $\delta^{18}O = ([^{18}O/^{16}O]_{sample}/^{18}[O/^{16}O]_{VSMOW} - 1) \times 1000$ (‰) and similarly for $\delta^{17}O$ using the $^{17}O/^{16}O$ ratio. $\Delta^{17}O$, which represents the deviation from the terrestrial fractionation line, has been calculated as: $\Delta^{17}O = \delta^{17}O - 0.52\ \delta^{18}O$ to compare our results for Vicência with those of Clayton et al. (1991). In terms of their oxygen-isotope compositions, ordinary chondrites are isotopically heterogeneous samples, and this is reflected in the variability in the replicate analyses of Vicência (Table 4). Figure 11 plots the mean oxygen isotopic composition of Vicência in relation to the ordinary chondrite analyses of Clayton et al. (1991) and shows that Vicência plots near the LL chondrite field.

Isotopic Composition of Secondary Fayalite

Oxygen Isotopic Composition

Oxygen isotopic compositions of secondary fayalite in Vicência are listed in Table 5, and on a three-isotope oxygen diagram, they plot along a mass-dependent fractionation line with a slope of ~0.5 and have an average $\Delta^{17}O$ of 4.0 ± 0.3‰ (2SD) (Fig. 12a). They are similar to those of secondary fayalite in the UOCs Elephant Moraine (EET) 90161, Meteorite Hills (MET) 96503, and Ngawi.

Manganese-Chromium Isotope Systematics

The Mn-Cr isotopic composition of secondary fayalite in Vicência are listed in Table 6, and Fig. 13 shows that excess ^{53}Cr is correlated with $^{55}Mn/^{52}Cr$, indicative of in situ decay of ^{53}Mn. The internal isochron for a ~40 × 40 μm fayalite grain has an initial $^{53}Mn/^{55}Mn$ ratio ($[^{53}Mn/^{55}Mn]_0$ of $[3.20 \pm 0.73] \times 10^{-6}$), corresponding to a formation age of $4.0^{+1.4}_{-1.1}$ Ma after CV CAIs when anchored to the quenched angrite D'Orbigny. The model isochron, defined using additional five fayalite grains, has an $(^{53}Mn/^{55}Mn)_0$ of $(3.21 \pm 0.65) \times 10^{-6}$, which also corresponds to a formation age of $4.0^{+1.2}_{-1.0}$ Ma after CV CAIs.

Long-Lived Cosmogenic Radionuclides

The concentrations of the long-lived cosmogenic radionuclides ^{10}Be and ^{26}Al in Table 2 were converted

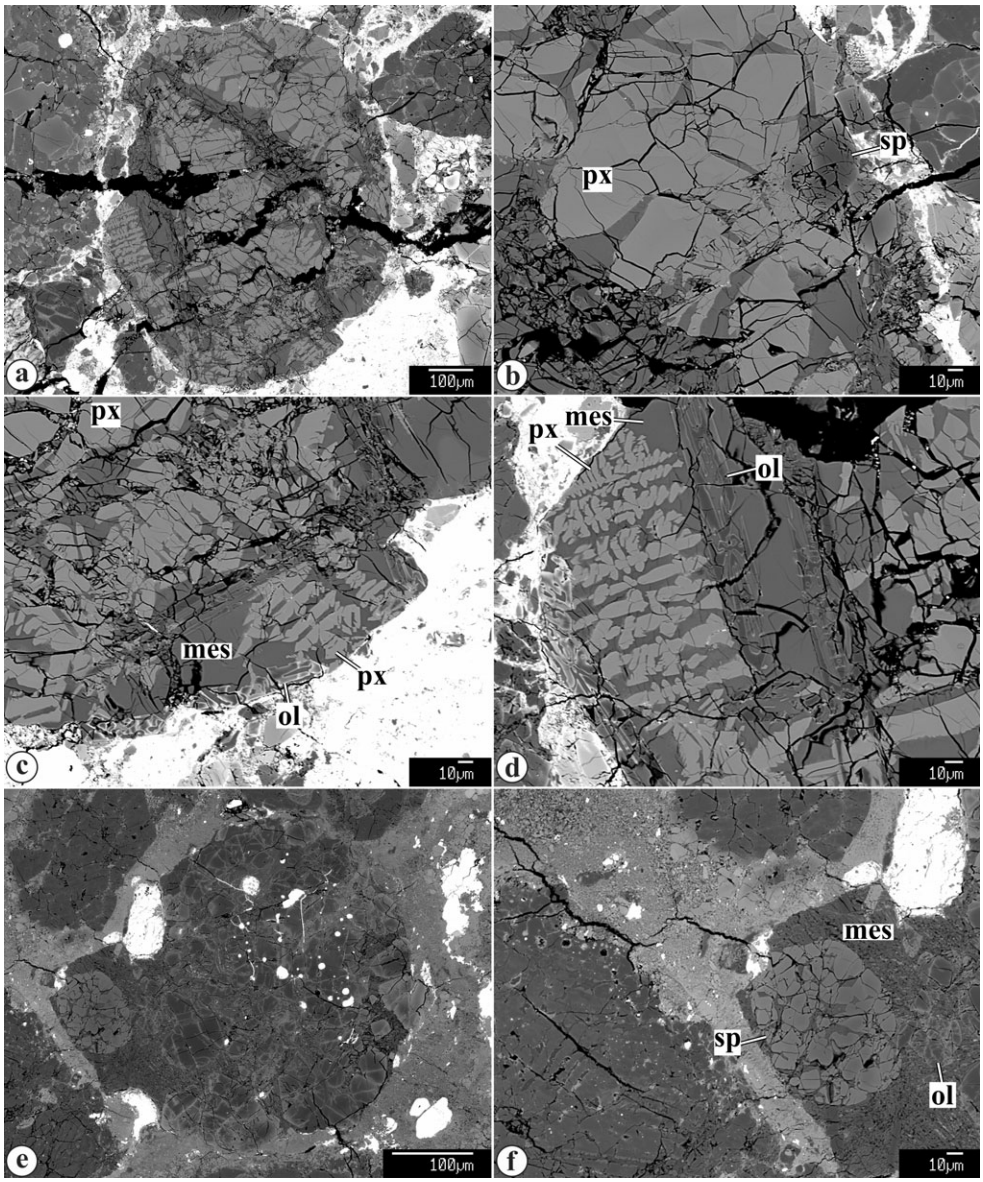

Fig. 4. Backscattered electron images of Al-rich chondrules from Vicência. a–d) Porphyritic chondrule (labeled as 3 in Fig. 2f) composed of coarse and skeletal crystals of high-Ca pyroxene (px), skeletal forsterite (ol), spinel (sp), and Na-rich glassy mesostasis (mes). e, f) Porphyritic olivine-pyroxene chondrule (labeled as 6 in Fig. 2f) containing a spinel-rich nodule.

from units of atoms per gram to units of disintegrations per minute per kg (dpm kg^{-1}). Reported values include analytical uncertainties in the AMS measurement of the samples, standards, and blanks, but not those in the absolute values of the standards.

Gamma Ray Measurements

The measured activities (corrected for radioactive decay since the time of fall) for the short-lived cosmogenic radionuclides (^{58}Co, ^{46}Sc, ^{57}Co, ^{54}Mn, ^{22}Na) and ^{26}Al are given in Table 7. For ^{60}Co and ^{44}Ti only upper detection limits are reported. The concentrations of U (11.8 ± 0.9 ng g^{-1}), Th (43.1 ± 3.3 ng g^{-1}), and K (935 ± 94 µg g^{-1}) were determined based on measured activities of the natural radionuclides ^{238}U, ^{232}Th, and ^{40}K of a 25.4 g specimen of Vicência. Errors include a 1σ uncertainty of ~10% in the detector efficiency calibration. The measured concentrations of U and Th are in good agreement with the average values for LL chondrites (Wasson and Kallemeyn 1988). The potassium concentration of 935 ± 94 ppm is higher than the average LL chondrite value of ~800 ppm, but in good agreement with the independent measurement of 1000 ± 50 ppm determined by ICP-OES (Table 2).

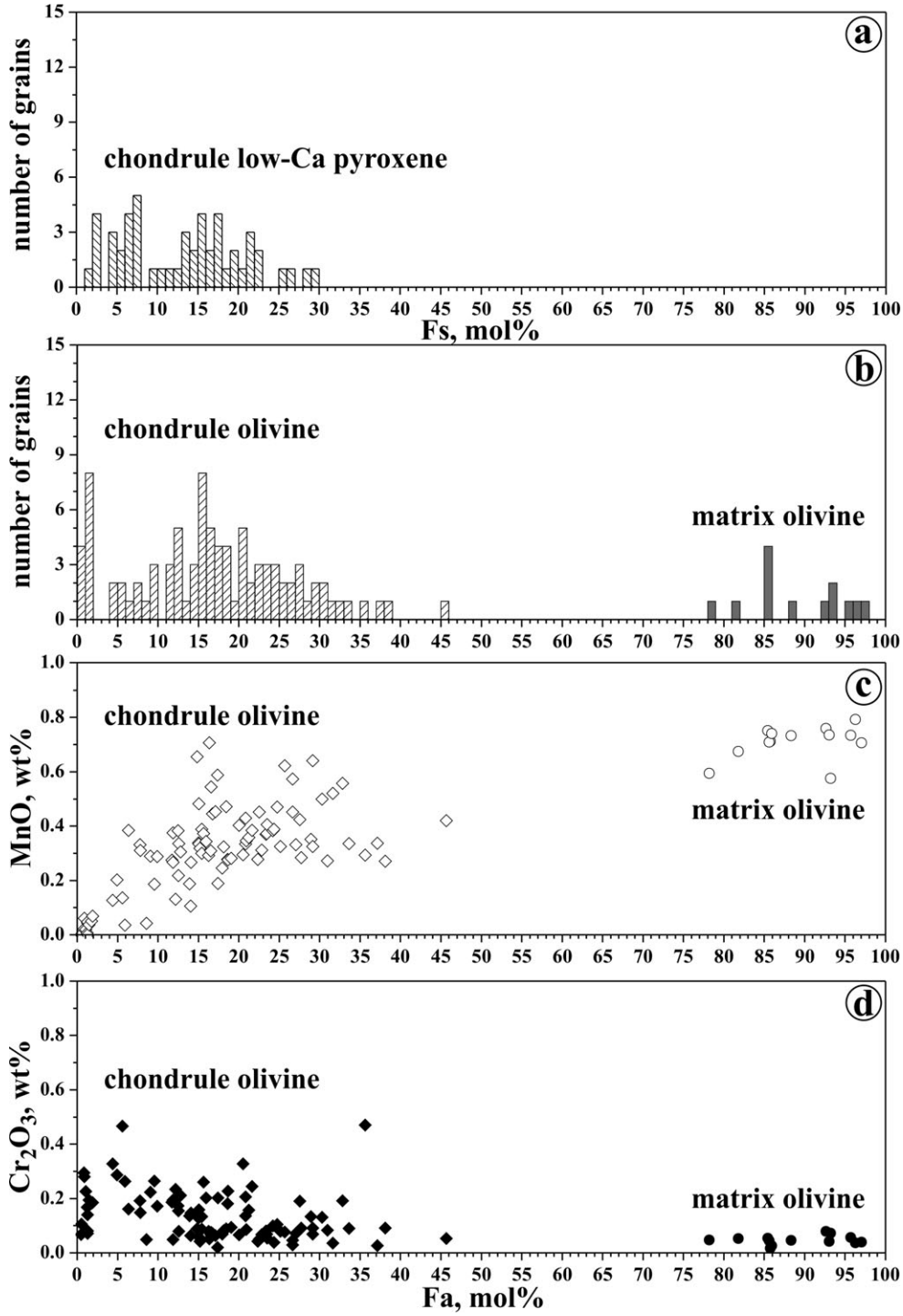

Fig. 5. Frequency distribution and compositions of olivine in chondrules and secondary fayalite (defined as $Fa_{>75}$) (here referred to as matrix olivine), and of low-Ca pyroxene in chondrules of Vicência. a) Fs content of low-Ca pyroxene in chondrules; b) Fa content, c) MnO content, and d) Cr_2O_3 content of olivine in chondrules and matrix.

Solar Modulation of Galactic Cosmic Ray flux

The activities of the short-lived radionuclides, half-lives of <11 yrs, are affected by solar activity, which modulates the galactic cosmic ray (GCR) flux by up to a factor of 2–3 within a solar cycle. As the production rates of short-lived radionuclides are both dependent on solar modulation and on shielding effects (as a function of size and depth within the meteoroid), it is difficult to

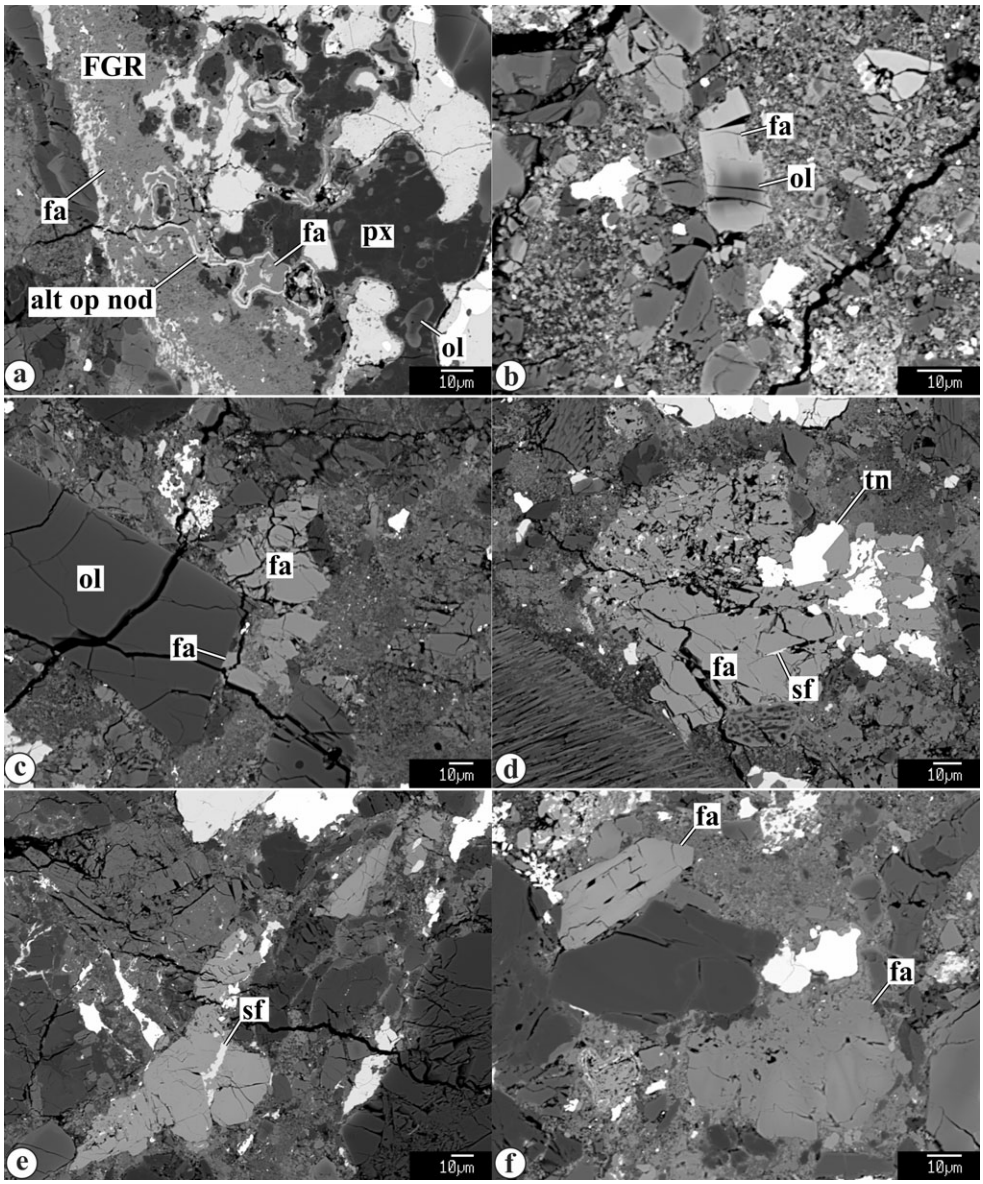

Fig. 6. Backscattered electron images of typical occurrences of secondary fayalite (fa; $Fa_{>75}$). It occurs as (a) small grains in fine-grained chondrule rims, (b, c) as overgrowths of olivine chondrule fragments, (c–f) and as coarse grains in the matrix. The coarse ferroan olivine grains often contain inclusions of taenite (tn) and sulfides (sf). Some of these grains show inverse compositional zoning, indicating postcrystallization Fe-Mg interdiffusion (see [f]). Occasionally, ferroan olivine replaces opaque nodules and low-Ca pyroxene in type I chondrule peripheries (see [a]). FGR = fine-grained rim; sf = secondary fayalite; alt op nod = altered opaque nodule; fa = fayalite; px = pyroxene; ol = olivine; tn = taenite.

disentangle these effects without performing detailed calculations of production rates as a function of shielding and solar modulation. As ^{22}Na and ^{26}Al are produced by similar low-energy reactions on Mg and Si, the $^{22}Na/^{26}Al$ production ratio is relatively independent of shielding effects so the $^{22}Na/^{26}Al$ activity ratio provides an empirical measure of solar modulation (e.g., Evans et al. 1982; Bhandari et al. 1993, 2002). The measured $^{22}Na/^{26}Al$ ratio of 1.63 ± 0.20 in Vicência is lower than values of 1.8–2.2 found in three chondrites (Jesenice, Mifflin, Novato) that fell between 2009 and 2012 (Bischoff et al. 2011; Kita et al. 2013; Jenniskens et al. 2014). The lower value for Vicência is consistent with its fall date in September 2013, near the maximum of the current solar cycle (number 24), resulting in a lower GCR flux than for meteorites that fell between 2009 and 2012. However, the $^{22}Na/^{26}Al$ ratio of 1.63 ± 0.20 for Vicência is intermediate between values of ~1 for high solar modulation (near solar maximum) and values of ~2 for low solar modulation (near solar minimum). This

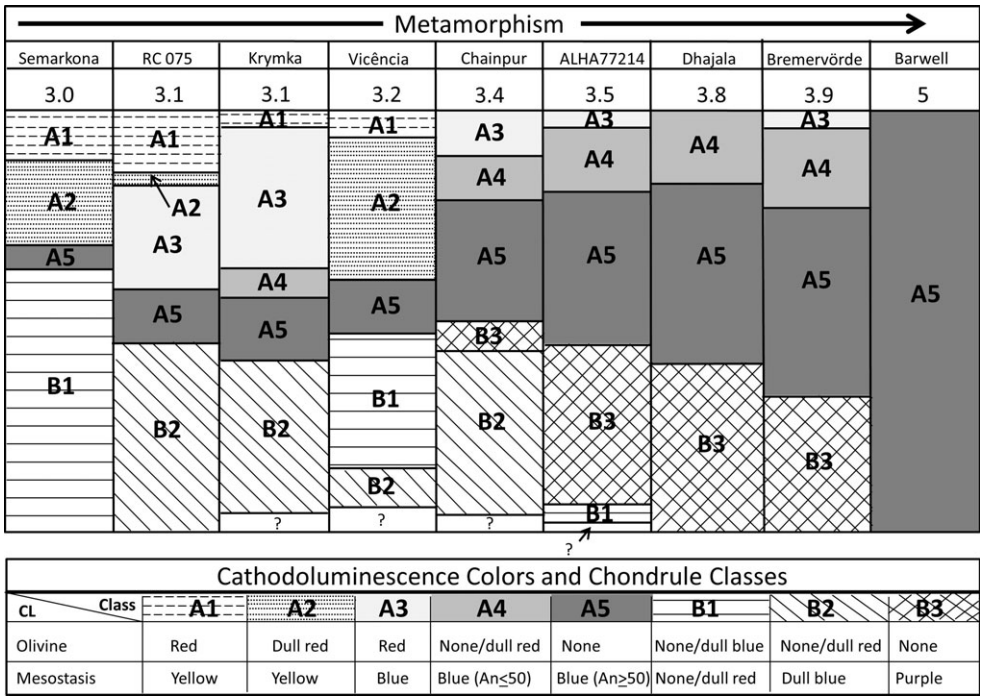

Fig. 7. Distribution of chondrules in % of their total numbers across the chemical classes (defined by Sears et al. 1992) for Vicência compared with similar data for nine ordinary chondrites (Sears et al. 1995). Clearly, Vicência is a low petrologic type meteorite, resembling Semarkona in its large number of B1, A1, and A2 chondrules, but a higher type suggested by the presence of B2 chondrules. The absence of A4 and B3 chondrules like in Chainpur precludes type 3.4. On balance, these data suggest type 3.1–3.3, consistent with 3.2.

intermediate $^{22}Na/^{26}Al$ ratio probably reflects the relatively low sunspot numbers (of ~60) in the current solar cycle, in addition to the long solar minimum that lasted from January 2007 till December 2009.

Preatmospheric Size of Vicência

To constrain the preatmospheric size of the Vicência meteorite, we compare the radionuclide concentrations with production rates from model calculations, which assume a constant GCR flux. Of the various cosmogenic radionuclides measured, we mainly use the ^{60}Co, ^{26}Al, and ^{10}Be data, as the production rates of these radionuclides are least affected by short-term variations in the GCR flux. ^{60}Co is the most sensitive to preatmospheric size and depth, as it is mainly produced by capture of low-energy secondary neutrons, which only occur in objects large enough (radius, $R > 20$ cm) to attenuate neutrons to thermal energies. For ^{60}Co in Vicência, only an upper limit of ~0.8 dpm kg^{-1} was determined, which is within the range of the expected production rate of 0.2–1 dpm kg^{-1} from spallation reactions via $^{60}Ni(n,p)^{60}Co$ and $^{62}Ni(n,p2n)^{60}Co$ (Spergel et al. 1986). This implies that Vicência contains no detectable neutron-capture ^{60}Co, indicating that the meteorite was most likely part of a meteoroid with $R < 20$ cm (Spergel et al. 1986). The alternative explanation that it was located very close (<1–2 cm depth) to the surface of a meteoroid with $R > 20$ cm is less likely, as this scenario would have produced elevated levels of ^{56}Co, a nuclide which is produced by solar cosmic rays (SCR), as was previously observed in a near-surface sample of the Sutter's Mill carbonaceous chondrite (Nishiizumi et al. 2014). The relatively low ^{10}Be (18.0 dpm kg^{-1}) and ^{26}Al (54.5 dpm kg^{-1}) concentrations are also consistent with production rates in LL chondrites with radii of 10–15 cm (Leya and Masarik 2009). This size corresponds to a preatmospheric mass of 13–45 kg, of which 3–9% survived atmospheric passage as a single fragment.

Noble Gases

The noble gas data are given in Table 8.

Cosmic Ray Exposure Ages

The ^{21}Ne and ^{38}Ar cosmic ray exposure (CRE) ages are calculated according to Dalcher et al. (2013), the ^{3}He age according to Eugster (1988), in all three cases using the $(^{22}Ne/^{21}Ne)_{cos}$ ratio of 1.19 to correct for shielding. The ^{21}Ne and ^{38}Ar ages agree with each other at 72 Ma, while the somewhat lower ^{3}He age of 58 Ma may indicate some loss of cosmogenic ^{3}He, as is also

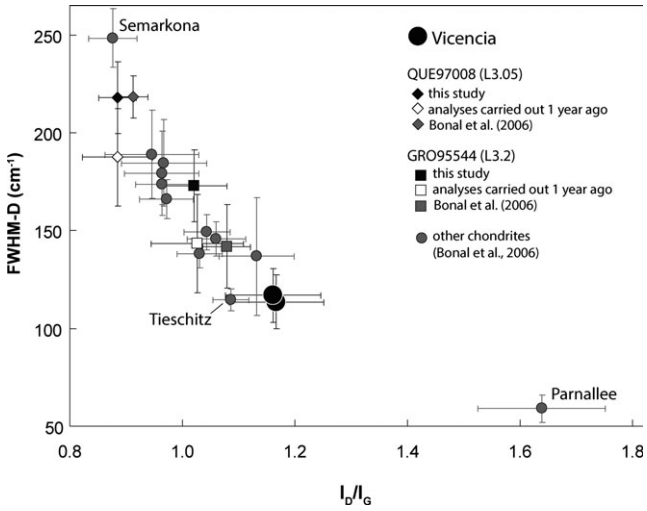

Fig. 8. FWHM-D versus I_D/I_G shows a correlation with metamorphic grade for ordinary chondrites. Analyses from this study indicate that Vicência is slightly more metamorphosed than GRO95544 (L3.2). Analyses of QUE97008 and GRO95544 done approximately 1 yr ago (laser power was 300 μW and total acquisition time was 150 s) are shown. They are consistent with analyses of this study. Analyses of QUE97008 and GRO95544 from Bonal et al. (2006) were collected using laser power of 500 μW and 540 s of acquisition time. They are also consistent with our analyses. Other ordinary chondrites analyzed by Bonal et al. (2006) are also shown. Some of the other chondrites have been labeled for reference. The uncertainties are 1σ.

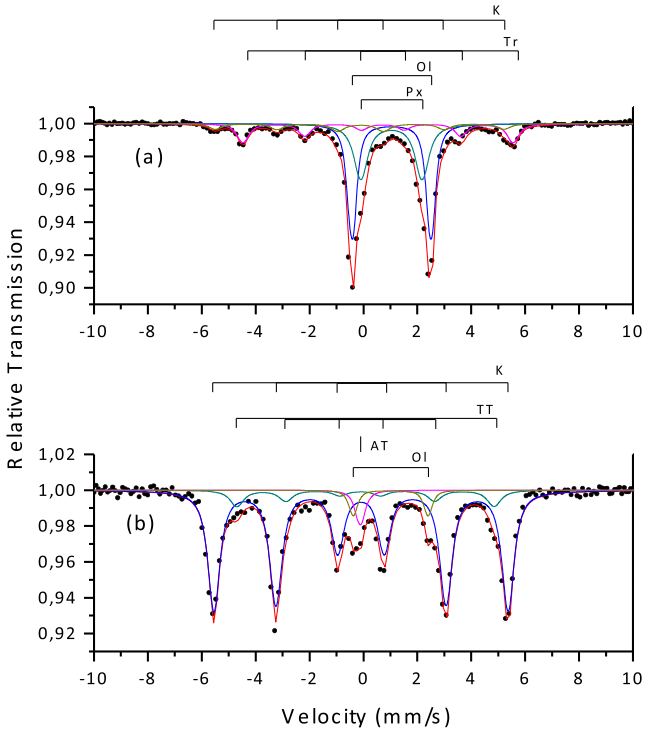

Fig. 9. ^{57}Fe Mössbauer spectra at room temperature for the Vicência (LL3.2) meteorite: a) bulk sample, b) metal particles extracted from a bulk sample. Identified phases: kamacite (K), tetrataenite (TT), antitaenite (AT), troilite (Tr), olivine (Ol), and pyroxene (Px).

indicated by the ^{3}He/^{21}Ne ratio, which falls ~15% below the correlation of ^{3}He/^{21}Ne versus ^{22}Ne/^{21}Ne (Eberhardt et al. 1966; Nishiizumi et al. 1980). The adopted CRE age of Vicencia of ~72 Ma (Table 8) is at the upper end of the age distribution observed for LL chondrites (Graf and Marti 1994; Scherer et al. 1998), in which only the CRE age of the LL4 chondrite Soko-Banja (71 Ma) is comparable to that of Vicência.

Primordial and Radiogenic Noble Gases

Measured ^{36}Ar, ^{84}Kr, and ^{132}Xe are almost entirely primordial. Concentrations are high, as expected for a highly unequilibrated chondrite. Figure 14 shows ^{132}Xe concentrations of a selection of bulk LL chondrite samples (compiled by Schultz and Franke 2004) as a function of their petrologic type. The data point for Vicência falls nicely along the trend defined by the ensemble of data and the trapped Xe concentration of Vicência is therefore well in line with its classification as LL3.2 chondrite. The isotopic compositions of Kr and Xe are typical for samples dominated by the noble gas component "Q" (Ott 2014), with some discernible contributions of cosmogenic Kr and Xe on the minor isotopes and likely a small isobaric interference on the ^{80}Kr signal.

Table 1. Mössbauer hyperfine parameters at room temperature for Vicência.

Mineral phase	δ (mm s^{-1})	Δ (mm s^{-1})	B_{hf} (T)	W (mm s^{-1})	A (%)
(a) Bulk					
Olivine	1.15	2.93	–	0.31	41
Pyroxene	1.15	2.27	–	0.55	31
Troilite	0.74	−0.18	31.1	0.47	18
Kamacite	−0.01	−0.02	33.2	0.54	10
(b) Metal particles					
Olivine	1.11	2.78	–	0.30	5
Kamacite	0.02	0.00	33.8	0.48	81
Tetrataenite	0.09	0.10	29.6	0.55	10
Antitaenite	−0.01	–	–	0.35	4

δ = isomer shift relative to α-Fe, Δ = quadrupole splitting, B_{hf} = hyperfine field, W = line width, A = relative area.

Radiogenic gas retention ages based on ^{40}Ar and ^{4}He are shown in Table 8. No attempt to correct for trapped primordial ^{4}He has been made; hence, the calculated U-Th-^{4}He age should be considered an upper limit. The nominal K-Ar age of 4.52 Ga is based on a K concentration of about 1000 ppm, the highest value measured for Vicência (Table 2). This age is within the

Table 2. Concentrations of major elements (in wt%) and K, Ti, and Co (in ppm) measured by ICP-OES of a 101.4 mg bulk sample of Vicência compared to average L and LL group ordinary chondrites (from Lodders and Fegley 1998; McSween and Huss 2010). In addition, given are the cosmogenic radionuclides ^{10}Be and ^{26}Al (in dpm kg^{-1}) for the sample of Vicência.

	Mg	Al	K	Ca	Ti	Mn	Fe	Co	Ni	^{10}Be	^{26}Al
Vicência	14.6	1.11	1000	1.28	650	0.24	17.0	370	0.83	18.0 ± 0.3	54.5 ± 0.6
Avg. L	14.9	1.16	900	1.33	670	0.259	21.8	580	1.24		
Avg. LL	15.3	1.18	880	1.32	680	0.26	19.8	480	1.06		

Table 3. Concentrations of 24 elements in Vicência determined by INAA. Mean data for LL chondrites from Wasson and Kallemeyn (1988).

	Na mg g^{-1}	K μg g^{-1}	Ca mg g^{-1}	Sc μg g^{-1}	Cr mg g^{-1}	Mn mg g^{-1}	Fe mg g^{-1}	Co μg g^{-1}	Ni mg g^{-1}	Zn μg g^{-1}	Ga μg g^{-1}	As μg g^{-1}
Vicência	6.96	889	13.4	9.39	4.16	2.62	200	500	10.2	49	5.4	1.39
Mean LL	7.00	790	13.0	8.40	3.74	2.62	185	490	10.2	46	5.0	1.35
	Se μg g^{-1}	Br μg g^{-1}	Ru μg g^{-1}	Sb ng g^{-1}	La ng g^{-1}	Sm ng g^{-1}	Eu ng g^{-1}	Yb ng g^{-1}	Lu ng g^{-1}	Os ng g^{-1}	Ir ng g^{-1}	Au ng g^{-1}
Vicência	10.1	0.45	0.85	48	360	212	82	257	41.6	451	400	133
Mean LL	9.9	0.6	0.68	60	315	200	76	220	33	400	360	

range of highest Ar-Ar ages on the order of 4.52 Ga observed in LL chondrites (Dixon et al. 2004; Bogard 2011). The nominal U-Th-^{4}He age of 3.58 Ga indicates some loss of radiogenic ^{4}He, which might have occurred late in the history of Vicência, possibly at the same time (in the last ~70 Ma) when cosmogenic ^{3}He was partly lost.

Thermoluminescence

The glow curve shape is very characteristic of meteorites of petrologic type 3.2, consisting of a very narrow peak and low glow curve temperatures. Ordinary chondrites of lower types (3.0–3.1) produce very broad hummocky peaks, because the amount of crystalline feldspar present is so low that many other phases compete in luminosity, the major competitors being the mesostasis of anorthositic and sodium-rich chondrules. Sears et al. (1992) referred to these chondrule types as A1 and A5, A1 being equivalent to the type I (refractory and reduced) chondrules, A5 being the unequilibrated version of chondrules in high petrographic types. Ordinary chondrites of higher petrographic types, type 3.5–3.9 have broad induced TL peaks at high glow curve temperatures. The TL sensitivity, peak temperature (T_p), and peak width (T_w) of two chips of Vicência are listed in Table 9, and the results are plotted in terms of thermoluminescence sensitivity relative to Dhajala = 1 versus petrologic type (Fig. 15a) and of peak temperature versus width of peak at half maximum (Fig. 15b). Both diagrams have become standard in reporting induced TL data in the context of metamorphic history and have been well-discussed (e.g., Sears et al. 1980, 2013; Guimon et al. 1985). Both TL peak shape and TL sensitivity suggest that Vicência is of petrologic type 3.2.

Magnetic Properties

Magnetic susceptibility (χ) and saturation magnetization (M_S) are proxies of the bulk metal content, and as such good indictors of the chemical group of ordinary chondrites. The magnetic susceptibility of Vicência is log χ = 4.30 (with χ in 10^{-9} m^3 kg^{-1}), in perfect agreement with the value log χ = 4.37 ± 0.24 of eight other LL3 falls, and below the log χ = 4.60 ± 0.11 of four L/LL falls (Rochette et al. 2003). Saturation magnetization is M_S = 6.64 Am^2 kg^{-1}, in agreement with the 4.11 ± 2.15 Am^2 kg^{-1} obtained on 28 LL falls, and 5.28 ± 2.02 Am^2 kg^{-1} obtained on five LL3 falls, and notably lower than the 17.51 ± 5.69 Am^2 kg^{-1} measured on five L/LL falls (Gattacceca et al. 2014).

Hysteresis properties are also good proxies of the metal mineralogy of ordinary chondrites. In particular, tetrataenite is readily identified because of its unusually high coercivity (e.g., Uehara et al. 2011). In this regard, Vicência stands out from other LL3 falls with a higher coercivity of remanence (B_{CR} = 290 mT), higher coercivity (B_C = 37 mT), and higher saturation magnetization (M_{RS} = 0.66 Am^2 kg^{-1}). Coercivity of remanence, the best proxy for the tetrataenite content, is 290 mT for Vicência compared to 75 ± 30 mT for five

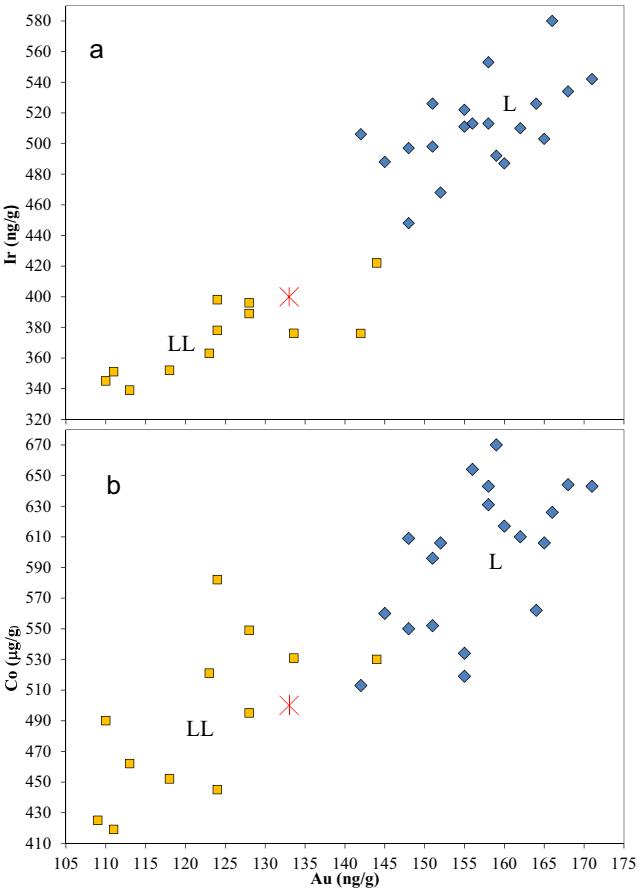

Fig. 10. Vicência data (the asterisks) are plotted on (a) Ir versus Au and (b) Co versus Au diagrams together with data for L and LL ordinary chondrites from Kallemeyn et al. (1989). Vicência plots near the upper end of the cloud of LL points but distinctly below the L field. This confirms that Vicência is an LL group ordinary chondrite.

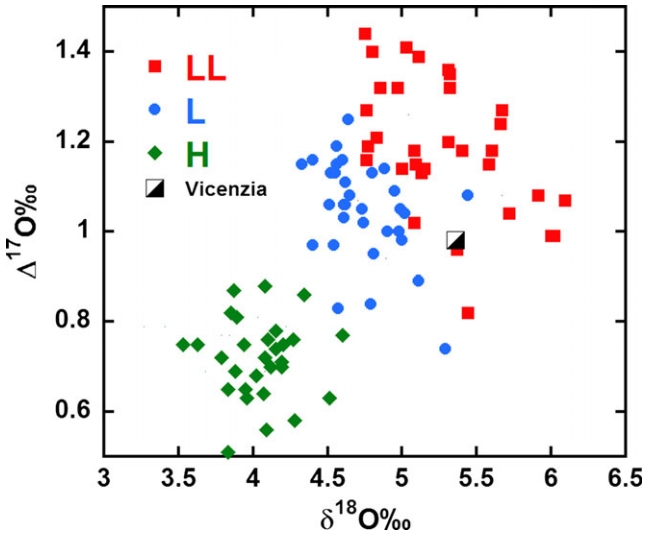

Fig. 11. Mean $\Delta^{17}O$ ($=\delta^{17}O - 0.52 \times \delta^{18}O$) versus $\delta^{18}O$ of the mean of three bulk samples of Vicência in relation to the bulk oxygen isotopic compositions of ordinary chondrites analyzed by Clayton et al. (1991).

Table 4. Oxygen isotopic composition of three chips of Vicência.

Date of run	$\delta^{17}O‰$	1σ	$\delta^{18}O‰$	1σ	$\Delta^{17}O‰$	1σ
11/20/13	3.772		5.362		0.984	
6/23/14-1	3.808		5.400		1.000	
6/23/14-2	3.725		5.316		0.961	
Mean	3.768	0.042	5.359	0.042	0.981	0.020

Table 5. Oxygen isotopic compositions of secondary fayalite in Vicência, obtained by in situ SIMS measurements.

Site	$\delta^{18}O‰$	2σ	$\delta^{17}O‰$	2σ	$\Delta^{17}O‰$	2σ
R4a-4@1	7.1	0.9	7.7	0.8	4.0	0.9
R31-1@1	9.4	0.8	8.8	0.8	3.9	0.9
R31-2@2	9.7	0.8	9.2	0.8	4.2	0.9
R69-2@1	9.9	0.9	9.1	0.9	4.0	1.0
R105-1@1	10.8	0.8	9.4	0.8	3.8	0.9
Average	9.4	0.8	8.8	0.8	4.0	0.9

other LL3 falls (Gattacceca et al. 2014). This indicates that a significant proportion of the metal in Vicência is tetrataenite. Using approximate values of $M_{RS}/M_S = 5 \times 10^{-3}$ for kamacite and 0.20 for tetrataenite in LL chondrites and Ms values of 224 $Am^2\ kg^{-1}$ for kamacite and 155 $Am^2\ kg^{-1}$ for tetrataenite (Gattacceca et al. 2014), the mass ratio of kamacite to tetrataenite in Vicência can be roughly estimated to be 4:1. Using this number allows estimating the bulk metal amount to ~3.5 wt% (~1.4 vol%). The acquisition of isothermal remanent magnetization (Fig. 16) confirms that tetrataenite is a major metallic mineral in Vicência, with the peak at 500 mT that can be correlated with tetrataenite in the cloudy zone of zoned taenite (Uehara et al. 2011). Evolution of magnetic susceptibility and saturation remanence with temperature does not show the Verwey transition at 120 K, diagnostic for the presence of magnetite (Fig. S10). Magnetite is detected in the most primitive LL3 chondrite falls Semarkona and Krymka, indicating significant aqueous alteration on the parent body. Although the composition of secondary fayalite in Vicência also indicates some degree of aqueous alteration, magnetite was not found by optical microscopy as well. The low temperature transition of chromite around 70 K (Gattacceca et al. 2011) is absent or very faint in Vicência, as observed in Krymka and Semarkona, in contrast to the more metamorphosed LL chondrites (Fig. S10).

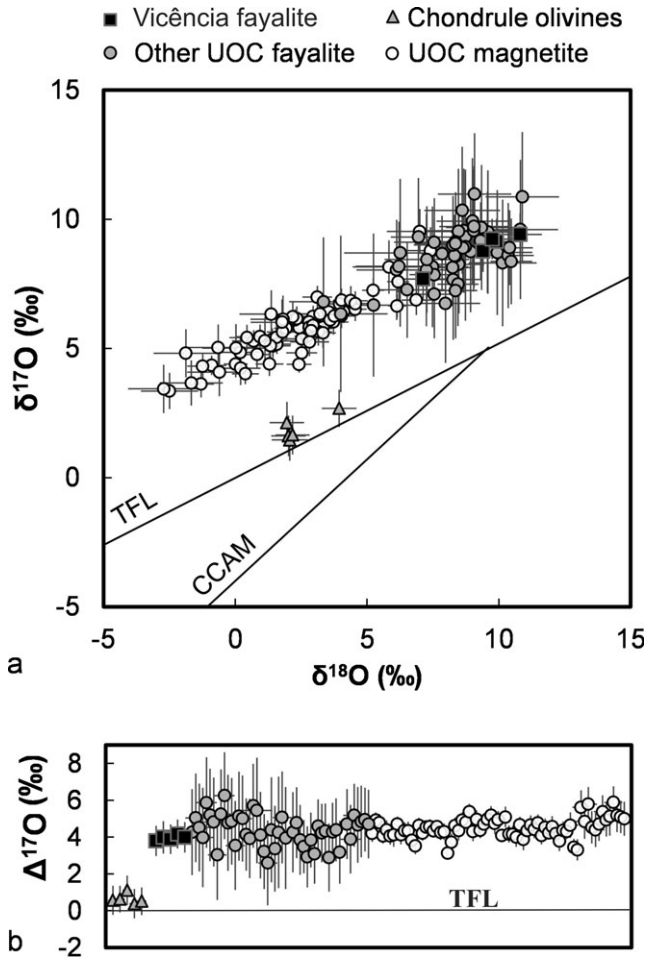

Fig. 12. a) A three-isotope oxygen diagram and (b) corresponding $\Delta^{17}O$ values for Vicência secondary fayalite shown together with oxygen isotopic compositions for secondary fayalite and magnetite from the unequilibrated ordinary chondrites (UOCs) Semarkona, EET 90161, MET 96503, MET 00452, and Ngawi (other UOC data from: Krot and Nagashima 2012; Doyle et al. 2014). The terrestrial fractionation line (TFL) and carbonaceous chondrite anhydrous mineral (CCAM) line are shown for reference.

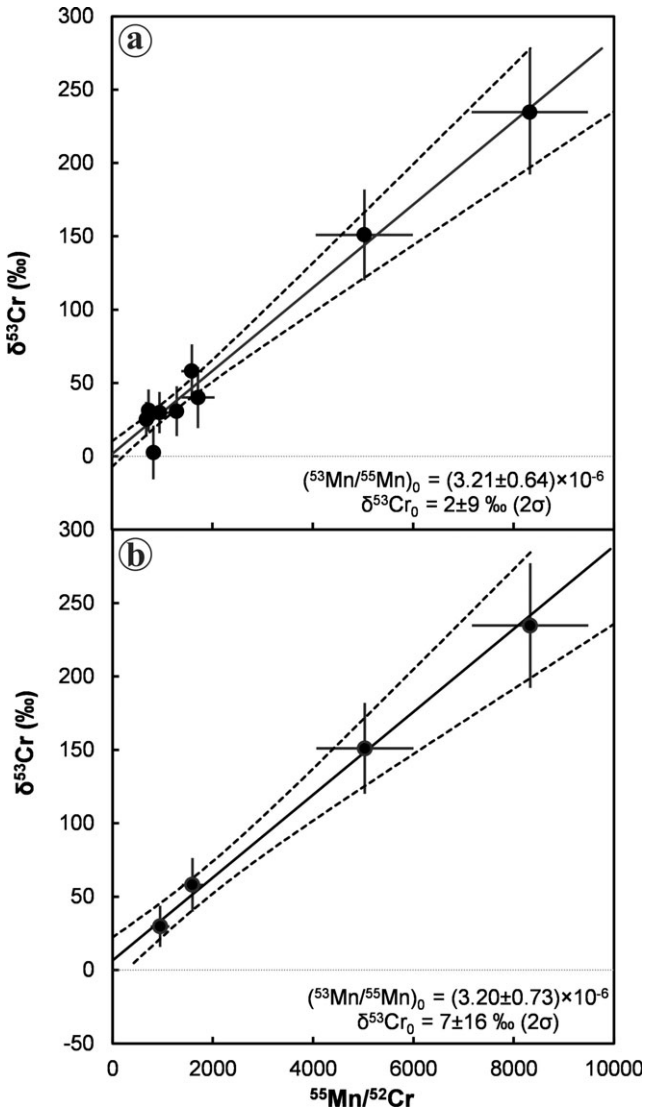

Fig. 13. ^{53}Mn-^{53}Cr evolution diagrams showing (a) the model, and (b) internal isochron for secondary fayalite in Vicência.

Table 6. Mn-Cr isotopic compositions of secondary fayalite in Vicência, obtained by in situ SIMS measurements.

Site	$^{55}Mn/^{52}Cr$	2σ	$^{53}Cr/^{52}Cr$	2σ	$\delta^{52}Cr$	2σ
R4a-1@1	1717	330	0.118	0.002	40	21
R31-4@1	1291	36	0.117	0.002	31	17
R39-2@1	686	91	0.116	0.001	25	12
R69-1@1	828	23	0.114	0.002	3	18
R100-1@1	734	46	0.117	0.002	31	14
R105-2@1	8327	1160	0.140	0.005	235	43
R105-3@2	1593	211	0.120	0.002	58	18
R105-n@3	5031	968	0.131	0.004	151	31
R105-n@4	950	187	0.117	0.002	30	14

Table 7. Massic activities (corrected to the time of fall) of cosmogenic radionuclides (in dpm kg^{-1}) in the 25.4 g specimen of Vicência measured by nondestructive gamma-ray spectroscopy. Errors include a 1σ uncertainty of ~10% in the detector efficiency calibration.

Nuclide	Half-life	Activity
^{58}Co	70.9 days	10 ± 5
^{46}Sc	83.8 days	12 ± 4
^{57}Co	271.8 days	4 ± 1
^{54}Mn	312.3 days	45 ± 5
^{22}Na	2.60 yrs	88 ± 8
^{60}Co	5.27 yrs	<0.79
^{44}Ti	60 yrs	<4.2
^{26}Al	7.05×10^5 yrs	54.2 ± 4.3

Table 8. Noble gases in Vicência.

Measured concentrations										Trapped and cosmogenic fractions			CRE ages (Ma)			Retention ages (Ga)	
^{3}He	^{4}He	^{20}Ne	^{21}Ne	^{22}Ne	^{36}Ar	^{38}Ar	^{40}Ar	^{84}Kr	^{132}Xe	$^{36}Ar_{tr}$	$^{38}Ar_{cos}$	$^{21}Ne_{cos}$	^{3}He	^{21}Ne	^{38}Ar	^{4}He	^{40}Ar
92.1	2168	18.1	17.0	20.3	58.6	13.1	8000	0.313	0.317	57	2.4	16.9	58	72	72	3.58	4.75
Kr isotopic composition ×100					Xenon isotopic composition ×100												
^{78}Kr/^{84}Kr	^{80}Kr/^{84}Kr	^{82}Kr/^{84}Kr	^{83}Kr/^{84}Kr	^{86}Kr/^{84}Kr	^{124}Xe/^{132}Xe	^{126}Xe/^{132}Xe	^{128}Xe/^{132}Xe	^{129}Xe/^{132}Xe	^{130}Xe/^{132}Xe	^{131}Xe/^{132}Xe	^{134}Xe/^{132}Xe	^{136}Xe/^{132}Xe					
0.64	4.82	20.67	20.32	30.41	0.464	0.414	8.10	112.5	16.03	81.38	37.67	31.67					

All concentrations (measured, trapped, and cosmogenic) are given in 10^{-8}cm^{3}STP g^{-1}. Uncertainties of concentrations are ~4%, uncertainties of Kr and Xe isotopic ratios are <1.5%. The ^{3}He cosmic ray exposure (CRE) age was calculated using Eugster (1988) and ^{21}Ne and ^{38}Ar CRE ages were calculated using equations provided by Dalcher et al. (2013), which yield ages that are 6–7% higher than those of Eugster (1988) for ^{21}Ne and Schultz et al. (1991) for ^{38}Ar. Nominal ^{4}He and ^{40}Ar retention ages were calculated using LL-chondritic chemistry (Lodders and Fegley 1998). In this calculation, all ^{40}Ar was assumed to be radiogenic. The ^{4}He was corrected for the cosmogenic contribution ($[^{4}He/^{3}He]_{cos}$ = 6.2), but not for a potential contribution from primordial ^{4}He carried by presolar grains.

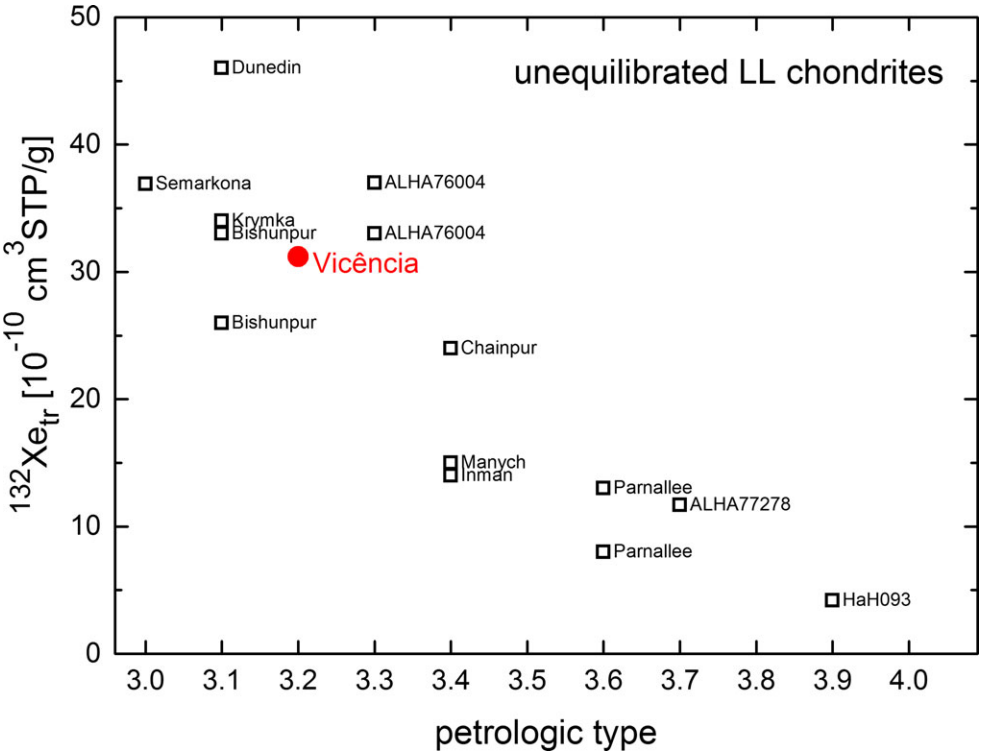

Fig. 14. Concentrations of trapped primordial ^{132}Xe in a selection of unequilibrated LL chondrite bulk samples of petrologic types 3.0–3.9, compiled by Schultz and Franke (2004). The concentration of trapped ^{132}Xe in Vicência supports its classification as an LL3.2 chondrite.

Table 9. The TL sensitivity, peak temperature (T_p), and peak width (T_w) of two chips of the Vicência chondrite. The uncertainty is 1σ on six measurements.

Sample	TL sensitivity. Dhajala = 1	T_p(°C)	T_w(°C)
264 mg chip	0.016 ± 0.003	126 ± 6	74 ± 2
408 mg chip	0.091 ± 0.0020	128 ± 5	77 ± 2

The bulk natural remanent magnetization (NRM) has the same direction in both samples (angular departure is 5°, below the orientation uncertainty). About 80% of the NRM is erased with an alternating field of 2 mT. Further demagnetization reveals component isolated between 4 and 24 mT in both samples. There is a 30° angle between the directions recovered from each sample, which is slightly higher than the orientation uncertainty. Above 24 mT, there is hardly any further demagnetization, and the end point directions differ by 125° between the two samples. Comparison with the demagnetization behavior of saturation isothermal remanent magnetization (sIRM) acquired in 3T is informative about the magnetizing field in which the NRM was created. The derivative ratio of NRM over sIRM (REM as defined in Gattacceca and Rochette 2004) integrated over this interval is ~1.5×10^{-4} in both samples, and the residual NRM over sIRM ratio are ~5×10^{-5}. This is typical of the behavior of LL chondrites, where the NRM, carried by tetrataenite, is spatially heterogeneous and likely acquired in a sub-null magnetic field and controlled by the crystalline anisotropy of tetrataenite (e.g., Gattacceca et al. 2003; Gattacceca and Rochette 2004).

High Resolution Mass Spectrometry Profiling of the Soluble Organic Compounds

Fourier transform ion cyclotron resonance mass spectrometry (FT-ICR-MS) was used to profile the methanol extractable organic matter of Vicência (Figs. S11 and S12). We detected the presence of a high chemical diversity (1845 CHNOS elementary compositions) in the range up to mass 700. Compared to this pristine LL3.2 Vicência, metamosphism as in the LL5 Chelyabinsk meteorite increased the chemical diversity to 2540 compositions. The described elementary compositions and chemical homologous series were found similar to those previously described in ordinary chondrites such as Chelyabinsk LL5 (Popova et al. 2013), Novato L6 (Jenniskens et al. 2014), or Soltmany L6 (Schmitt-Kopplin et al. 2012), with mainly CHO- and

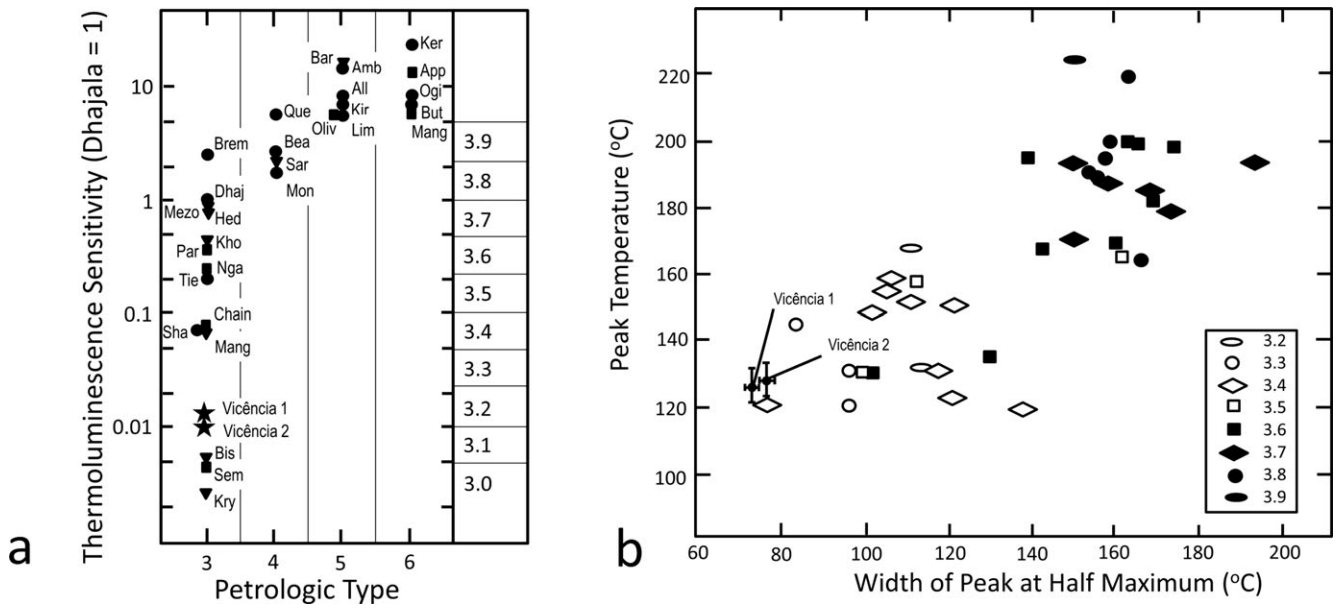

Fig. 15. Induced thermal luminescence a) plotted in terms of thermoluminescence sensitivity relative to Dhahala = 1 versus petrologic type, for two chips of the Vicência chondrite, suggesting petrologic type 3.2 classification. The abbreviations for comparative meteorites are type 3: Kry, Krymka; Bis, Bishunpur; Sem, Semarkona; Man, Manych; Sha, Sharps; Chain, Chainpur; Tie, Tieschitz; Nga, Ngawi; Par, Parnallee; Koh, Khohar; Hed, Hedjaz; Mezo, Mezö-Madaras; Dhaj, Dhajala; Brem, Bremervörde. Type 4: Mon, Monroe; Sar, Saratov; Bea, Beaver Creek; Que, Quenggouk. Type 5: Oliv, Olivenza; Lim, Limerick; Kir, Kirin (Jilin); All, Allegan; Amb, Ambapur Nagla; Bar, Barwell. Type 6: Mang, Mangwendi; But, Butsura; Ogi, Ogi; App, Appley Bridge; Ker, Kernouve. The symbols are square, LL; triangle, L; circle, H group chondrites. b) Induced thermal luminescence plotted in terms of peak temperature versus width of peak at half maximum, for two chips of the Vicência chondrite, suggesting petrologic type 3.2 classification.

CHOS-type of molecular composition. Higher metamorphism such as in Kilabo LL6 significantly altered the compositional profile (reduction to only 680 compositions).

DISCUSSION

Chemical Group

Based on the data obtained in this study, we conclude that the Vicência UOC belongs to the LL chemical group.

For example, the bulk density of Vicência of 3.13 g cm^{-3} is close to the average bulk density of LL group meteorite falls of 3.22 ± 0.22 (Consolmagno et al. 2008), suggesting the meteorite belongs in the LL chemical group. However, the grain density of 3.28 g cm^{-3} and porosity of 4.75% are slightly different from those for LL meteorite falls of 3.54 ± 0.13 and 8.2 ± 5.50%. In addition, while the chondrules in Vicência vary in apparent diameter from ~0.2 to 2.8 mm, we estimate, by deleting six very large chondrules, that the mean chondrule diameter approximates 0.9 mm, identical to the mean apparent diameter of chondrules in LL group chondrites (Grossman et al. 1988; Krot et al. 2014). A. Rubin (personal communication) pointed out to us that these earlier data have been superseded by the work of Nelson and Rubin (2002), who measured the sizes of 719 intact chondrules from LL chondrites and found a mean size of 570 μm. The very extensive compilation of essentially all reported chondrule sizes of ordinary chondrites by Friedrich et al. (2015) shows considerable in-group variability of chondrule diameters, suggesting that this may not be a reliable classification parameter. LL group classification is indicated by the content of 1–2.4 vol% (average 1.8 vol%) of metallic Fe, Ni determined by modal analyses and of ~3.5 wt% (1.4 vol%) indicated by the magnetic hysteresis properties and Mössbauer spectroscopy, which is close to that of average LL group chondrites of 2.0 vol% (Krot et al. 2014). The Co content of kamacite of 1.73 ± 0.3 wt%, while particularly useful for classifying equilibrated chondrites, is also consistent with LL group classification (Rubin 1990). The bulk oxygen isotope composition of $\delta^{17}O$ = 3.768 ± 0.042‰, $\delta^{18}O$ = 5.359 ± 0.042‰, $\Delta^{17}O$ = 0.981 ± 0.020‰, is also close to that of LL group ordinary chondrites.

Determination of the chemical group, particularly of low-petrologic type UOC, based on their bulk chemical compositions, has been notoriously difficult as, for example, shown by Jarosewich and Dodd (1981). They point out that element ratios rather than absolute

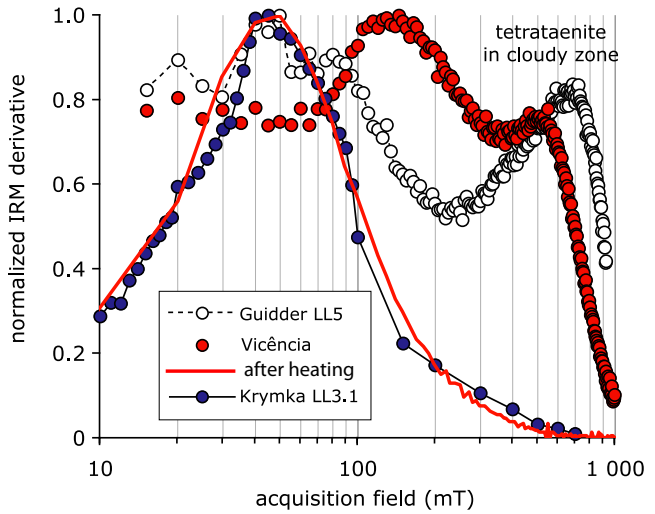

Fig. 16. Derivative of the isothermal remanent magnetization (IRM) as a function of applied magnetic field for Guidder, Krymka, and Vicência. The latter was also measured after a thermal treatment which served to disorder tetrataenite. Each peak represents a ferromagnetic mineral. Specifically, the peak at 500 mT for Vicência corresponds to tetrataenite in the cloudy zone of zoned taenite grains.

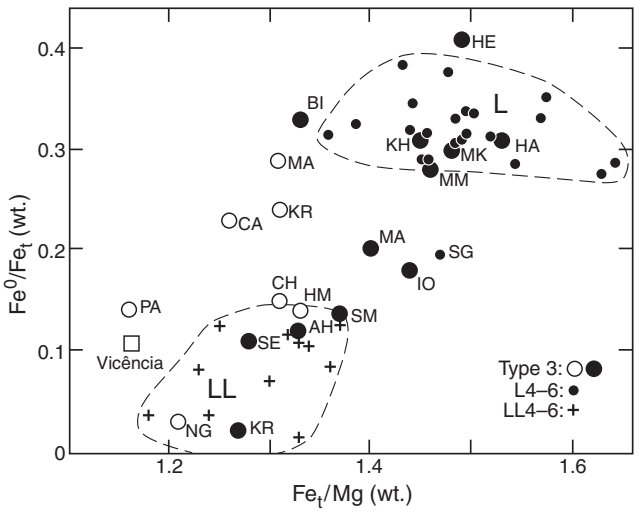

Fig. 17. The bulk meteorite ratios of metallic iron over total iron (Fe^0/Fe_t) plotted versus the ratios of total iron over magnesium (Fe_t/Mg) in L and LL group ordinary chondrites. For clarity, fields of equilibrated ordinary chondrites are outlined by dashed lines. One L6 chondrite, Segowlie, lies well outside the L4–6 field and is labeled (SG). Type 3 chondrite analyses by Jarosewich (1990) are indicated by filled circles, and those by other analysts by open circles. Not all meteorite data points are labeled. Those that are include Hedjaz (HE), Bishunpur (BI), Khohar (KH), Mabwe Khoywa (MK), Hallingeberg (HA), Manych (MA), Mezö-Madaras (MM), Krymka (KR), Carraweena (CA), Ioka (I0), Chainpur (CH), Hamlet (HM), Parnallee (PA), St. Mary's County (SM), Allan Hills 77278 (AU), Semarkona (SE), and Ngawi (NG). Vicência plots very near the LL and far away from the L group fields. (Modified from Jarosewich and Dodd [1981], and reprinted with permission from the Meteoritical Society.)

values may actually be better for assigning a chondrite to either the L or LL groups. The ratios of metallic Fe^0/total iron (0.105) versus total Fe/Mg (1.164) and of Ni/Mg (0.057) versus total Fe/Mg for Vicência (Table 2) plot in or very close to the LL fields of Jarosewich and Dodd (Figs. 17 and 18).

Finally, the siderophile elements Co, Ir, and Au in Fig. 10 (and supported by our data for other siderophiles such as Ni and Fe) show that Vicência is an LL ordinary chondrite.

Petrologic Type

All data obtained in this study indicate that Vicência is an UOC of petrologic type 3.2

As shown by Grossman and Brearley (2005), a plot of the standard deviation versus the mean Cr_2O_3 content (in wt%) of ferroan olivine in ordinary chondrites allows determination of the petrologic type of low-petrologic type 3 ordinary chondrites. As Fig. 19 shows, Vicência, with a Cr_2O_3 content in olivine of ~0.14 wt% and a standard deviation of ~0.09, is a petrologic type 3.2 ordinary chondrite. The TL sensitivity (induced TL at peak emission divided by the same quantity for the Dhajala [H3.8] chondrite, Fig. 15a) is a reflection of the degree of crystallization of feldspar, it being the mineral responsible for the TL of all but the least metamorphosed ordinary chondrites (Sears et al. 1980). The temperature of the major TL emission peak, and the width of this peak (Fig. 15b), depend on the form of the feldspar, whether it is in the low-temperature (ordered) or in the high-temperature (disordered) structural form (Guimon et al. 1984, 1985). The order–disorder transformation for oligoclase (the composition of ordinary chondrite feldspar) is 500–600 °C (McKie and McConnell 1963). Comparison to literature data on TL sensitivity of ordinary chondrites of known petrologic type indicates that Vicência is a type 3.2 UOC (Fig. 15a), and so does the peak temperature and peak width at half maximum (Fig. 15b).

It should be noted that Vicência has the most narrow and lowest temperature peak yet observed in ordinary chondrites (Fig. 15b). It is known that the width of the TL peak in ordinary chondrites is governed by the relative proportions of low- and high-temperature feldspar. Most ordinary chondrites contain a mixture of feldspar types, which was determined by peak metamorphic temperatures and cooling rates. The TL peak shape for Vicência suggests that the feldspar is in the low-temperature form and remarkably pure.

The composition of the chondrules (particularly of olivine and mesostasis) is reflected in their cathodo-

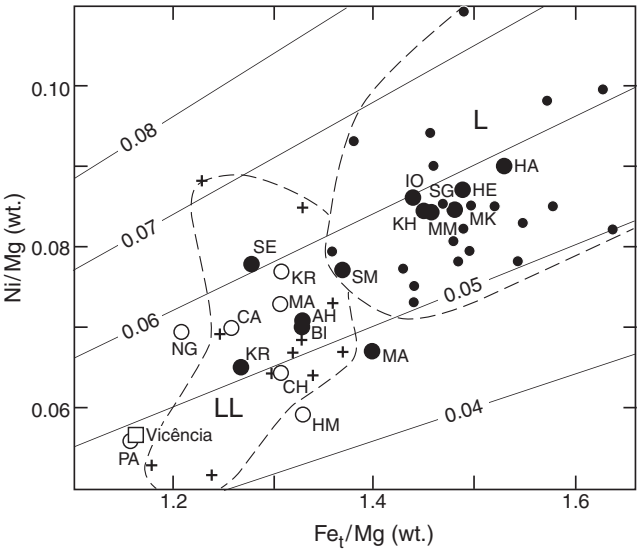

Fig. 18. The bulk meteorite ratios of nickel over magnesium (Ni/Mg) plotted versus the ratios of total iron over magnesium (Fe_t/Mg) in L and LL group ordinary chondrites. For clarity, fields of equilibrated ordinary chondrites are outlined by dashed lines. Not all meteorite data points are labeled but those that are labeled are like in Fig. 17, and so are the symbols. Vicência plots very near the LL and far away from the L group fields. (Modified from Jarosewich and Dodd [1981], and reprinted with permission from the Meteoritical Society.)

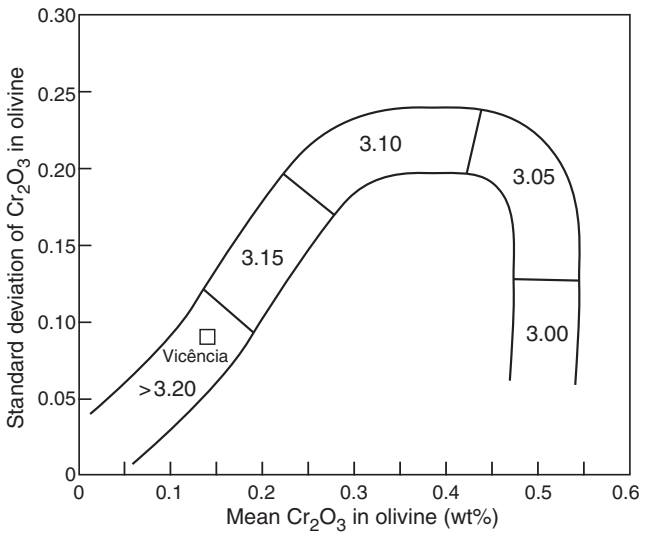

Fig. 19. Plot of the standard deviation versus the mean Cr_2O_3 content (in wt%) of ferroan olivine in ordinary chondrites. For clarity, the individual meteorites, upon which this diagram is based, are not plotted, but the fields of petrologic types and the parallel lines denoting the approximate spread of points are shown. Suggested divisions for subdividing the low-petrologic type 3 chondrites are also shown, indicating that Vicência, with a mean Cr_2O_3 content of ~0.14 wt% and a standard deviation of ~0.09, is a petrologic type 3.2 ordinary chondrite (diagram modified from Grossman and Brearley [2005], and published with permission from Elsevier).

luminescence properties (Fig. 7). The metamorphism-related trends in CL properties were described by Sears et al. (1992, 1995) and DeHart et al. (1992). In Semarkona, chondrules were separated into those that luminesce (group A) and those that do not (group B), which are also (to a good approximation) the FeO-poor and FeO-rich chondrules of previous classification schemes (beginning with Wood 1967). As metamorphism progresses, both groups A and B undergo compositional and physical changes which affect their CL properties and give rise to seven subgroups; A1–A4 and B1–B3 (see Fig. 7 for details of the CL colors of olivine and mesostasis). Additionally, there is a group of chondrules (A5) that have the composition of the chondrules of equilibrated chondrites; the only change they experience during metamorphism is homogenization of their mineral compositions. The result is that both the A and B groups converge on A5 (A1→A2→A3→A4→A5 and B1→B2→B3→A5) as metamorphism reaches type 5 and 6 levels (Sears et al. 1995, 2013).

Thus, in Fig. 7, there are several trends in chondrule group populations with increasing metamorphism. In Semarkona, only 5% are group A5. With increasing metamorphism, as the original A5 chondrules homogenize, the group proportion increases as group A and B chondrule compositions change and convert to group A5. Group A1 and A2 are only seen in very low petrologic types 3.0–3.2. Group A4 are only seen in any abundance in the high petrologic types (say 3.5–3.9). The group B1 chondrules are (essentially) only seen in petrologic type 3.0, and type B3 only in high petrologic types 3.5–3.9. Thus, the chondrule population is a sensitive indicator for the petrologic type of chondrites. In its abundance of large numbers of group A1, A2, and B1 chondrules, Vicência resembles Semarkona, but the presence of B2 chondrules places Vicência higher in the metamorphic scale, but the absence of B3 and A4 chondrules places Vicência at a type below 3.4. On the basis of these data, Vicência would seem to be type 3.1–3.3. This is a fairly conservative estimate, based on the limited number of Vicência chondrules, the limited number of meteorites for comparison, and that CL data from a microprobe are being compared with CL data from a luminoscope. However, the CL data for Vicência are consistent with petrologic type 3.2.

Figure 14 shows the relationship between trapped $^{132}Xe_{tr}$ and petrologic type for unequilibrated LL group chondrites. The concentration of $^{132}Xe_{tr}$ in Vicência is entirely consistent with its classification as petrologic type 3.2. Within uncertainties, Raman spectroscopy of the carbonaceous matrix of Vicência (Fig. 8) also supports this classification.

Finally, it should be noted that the high tetrataenite content (Fig. 9) is unusual for what is observed in other LL3 meteorites. Formation of tetrataenite requires slow cooling below 320 °C (the disordering temperature of tetrataenite), ideally starting from higher temperatures (~400 °C but this is particularly unconstrained), when Ni diffusion is fast enough to allow Ni to concentrate in the metal. "Tetrataenite," together with awaruite, is sometimes described as an aqueous alteration product in the most primitive chondrites (e.g., Brearley and Krot 2013). But as acknowledged, for instance, by Rambaldi and Wasson (1984), who describe tetrataenite in Krymka, this is based only on elemental composition and the ordering of this "tetrataenite" is not confirmed, so it should rather be called (Ni-rich) taenite. In the most primitive ordinary chondrites this is confirmed by the much lower coercivity of remanence compared to more metamorphosed ones (Gattacceca et al. 2014), indicating that there is no significant tetrataenite contribution. In Vicência, the high nickel metal is ordered and therefore likely not from aqueous alteration origin, but from thermal origin. This paradox is illustrated in Fig. 16, where Vicência and Guidder (a tetrataenite rich LL5) both display a very high coercivity peak around 500–600 mT that is absent in Krymka. We submitted Vicência to a thermal treatment at 475 °C for 20 h to disorder tetrateanite (Dos Santos et al. 2015). After tetrataenite disordering, Vicência displays a coercivity spectrum remarkably similar to the one of Krymka (Fig. 16). This is in agreement with the absence in Vicência of magnetic aqueous alteration products like magnetite that can be detected by magnetic measurements, for instance, in Semarkona and Krymka. The abundance of tetrataenite in Vicência implies a different thermal history compared to other LL3 chondrites. Either the meteorite was heated to higher temperatures than commonly accepted for a type 3.2 chondrite, or cooling from the peak metamorphism temperature was significantly slower than usual. More work is underway, including magneto-optical imaging (see e.g., Uehara et al. 2011) to resolve the spatial distribution of tetrataenite that may help clarify its formation process.

Mössbauer studies of Vicência indicate that, like in other ordinary chondrites, the Fe-bearing phases consist of olivine, pyroxene, troilite, and Fe-Ni metal (Fig. 9). Iron oxides of terrestrial origin were not detected, as would be expected in a fresh fall. The analysis of the metal indicates kamacite and tetrataenite as the main Fe-Ni phases. Kamacite (K) is present in a higher relative proportion than tetrataenite (TT) (Table 1). According to the ^{57}Fe-MS results of the metal, the relative proportion of K and TT is 80% and 10%, respectively, considering only the Fe content. Taking into account the molecular formula of each phase, the proportion K:TT is 4:1 (wt%), in agreement with the estimates derived from magnetic hysteresis properties.

Previous works (Danon et al. 1979) on ordinary chondrites show that the quadrupole splitting (Δ) of tetrataenite, measured by Mössbauer spectroscopy, indicates its ordering degree as well as the cooling rate below its order–disorder transition temperature (~320 °C). The ordering degree of tetrataenite ($\Delta \sim 0.10$ mm s^{-1}) from Vicência, a nonshocked sample with metamorphic grade 3.2, suggests slow cooling below 320 °C. However, it seems that other LL chondrites with higher metamorphic grade experienced slower cooling rates than Vicência.

Formation of Secondary Fayalite During Low-Temperature Aqueous Alteration on the Vicência LL Chondrite Parent Body

The oxygen isotopic compositions of secondary fayalite in Vicência plot along a mass-dependent fractionation line with a slope of ~0.5 and have an average Δ^{17}O of 4.0 ± 0.3‰, similar to those of secondary fayalite in the unequilibrated chondrites EET 90161, MET 96503, and Ngawi (Fig. 12a) which have an average Δ^{17}O of 4.5 ± 1.7‰ (Krot and Nagashima 2012; Doyle et al. 2014). The oxygen isotopic composition of secondary fayalite in Vicência suggests that it was in equilibrium with a fluid with a Δ^{17}O of ~+4‰, consistent with the composition of the fluid which was in equilibrium with secondary magnetite and fayalite in other UOCs (Krot and Nagashima 2012; Doyle et al. 2014).

The oxygen isotopic compositions of fayalites in Vicência are well resolved from those of chondrule olivines from EET 90161 (Fig. 12b), which have an average Δ^{17}O of 0.6 ± 0.1‰ (2SD). Secondary fayalite and the chondrule olivine phenocrysts in Vicência are not in isotopic equilibrium, consistent with low-temperature formation of fayalite during aqueous alteration on the UOC parent body.

Age of Aqueous Alteration of the Vicência LL Chondrite Parent Body

Manganese-chromium systematics establish the age of formation of secondary fayalite in Vicência of $4.0^{+1.4}_{-1.1}$ Ma after CV CAIs, when anchored to the D'Orbigny angrite. It dates the age of aqueous alteration on the LL chondrite parent body (Fig. 13). This appears to be younger than that for fayalites in EET 90161 ($2.4^{+1.8}_{-1.3}$ Ma after CV CAIs; Doyle et al. 2014), although the ages are not resolved with uncertainties of our measurements. Interestingly, the age of fayalite in Vicência is very similar to the age of fayalite in Asuka 881317 (CV3), dated to be $4.2^{+0.8}_{-0.7}$ Ma after CV CAIs (Doyle et al. 2013).

Acknowledgments—The research of ANK, PMD, TVK, MT, and KK was supported in part by grant NNX10AH76G from the NASA Cosmochemistry Program (A. N. Krot, PI), that of JTW by NASA grant NNX10AG98G, that of KW by the NASA Cosmochemistry Program, and that of MR and RW by the Swiss National Science Foundation. DWGS is grateful to Chris McKay for support and Hazel Sears for assistance in the laboratory. The TL laboratory is supported by a SSERVI grant to the FINESSE project (PI: Jennifer Heldmann). We thank Alan Rubin, Addi Bischoff, and an anonymous reviewer for most valuable and constructive comments that have improved the manuscript considerably. "This is Hawai'i Institute of Geophysics and Planetology publication number 2169 and School of Ocean and Earth Science and Technology publication number 9424".

Editorial Handling—Dr. Gretchen Benedix

REFERENCES

Bhandari N., Mathew K. J., Rao M. N., Herpers U., Bremer K., Vogt S., Wölfli W., Hofmann H. J., Michel R., Bodemann R., and Lange H.-J. 1993. Depth and size dependence of cosmogenic nuclide production rates in stony meteoroids. *Geochimica et Cosmochimica Acta* 57:2361–2375.

Bhandari N., Murty S. V. S., Shukla P. N., Shukla A. D., Mahajan R. R., Sarin M. M., Srinivasan G., Suthar K. M., Sisodia M. S., Jha S., and Bischoff A. 2002. Itawa Bhopji (L3-5) chondrite regolith breccia: Fall, classification and cosmogenic records. *Meteoritics & Planetary Science* 37:549–563.

Bischoff A., Jersek M., Grau T., Mirtic B., Ott U., Kučera J., Horstmann M., Laubenstein M., Herrmann S., Randa Z., Weber M., and Heusser G. 2011. Jesenice—A new meteorite fall from Slovenia. *Meteoritics & Planetary Science* 46:793–804.

Bogard D. D. 2011. K-Ar ages of meteorites: Clues to parent-body thermal histories. *Chemie der Erde—Geochemistry* 71:207–226.

Bonal L., Quirico E., Bourot-Denise M., and Montagnac G. 2006. Determination of the petrologic type of CV3 chondrites by Raman spectroscopy of included organic matter. *Geochimica et Cosmochimica Acta* 70:1849–1863.

Bonal L., Bourot-Denise M., Quirico E., Montagnac G., and Lewin E. 2007. Organic matter and metamorphic history of CO chondrites. *Geochimica et Cosmochimica Acta* 71:1605–1623.

Brearley A. J. and Krot A. N. 2013. Metasomatism in the early solar system: The record from chondritic meteorites. In *Metasomatism and the chemical transformation of rock, Lecture notes in earth system sciences*, edited by Harlov D. E. and Austrheim H. Berlin: Springer-Verlag. pp. 659–789.

Clayton R. N., Mayeda T. K., Goswami J. N., and Olsen E. J. 1991. Oxygen isotope studies of ordinary chondrites. *Geochimica et Cosmochimica Acta* 55:2317–2333.

Consolmagno G. J., Britt D. T., and Macke R. J. 2008. The significance of meteorite density and porosity. *Chemie der Erde/Geochemistry* 68:1–29.

Dalcher N., Caffee M. W., Nishiizumi K., Welten K. C., Vogel N., Wieler R., and Leya I. 2013. Calibration of cosmogenic noble gas production in ordinary chondrites based on ^{36}Cl-^{36}Ar ages. Part 1: Refined produced rates for cosmogenic ^{21}Ne and ^{38}Ar. *Meteoritics & Planetary Science* 48:1841–1862.

DeHart J. M., Lofgren G. E., Lu J., Benoit P. H., and Sears D. W. G. 1992. Chemical and physical studies of chondrites—X: Cathodoluminescence studies of metamorphism and nebular processes in type 3 ordinary chondrites. *Geochimica et Cosmochimica Acta* 56:3791–3807.

Dixon E. T., Bogard D. D., Garrison D. H., and Rubin A. E. 2004. ^{39}Ar-^{40}Ar evidence for early impact events on the LL chondrite parent body. *Geochimica et Cosmochimica Acta* 68:3779–3790.

Danon J., Scorzelli R. B., Souza Azevedo I., and Michel-Levy M. C. 1979. Iron-nickel superstructure in metal particles of chondrites. *Nature* 281:469–471.

Dos Santos E., Gattacceca J., Rochette P., Fillion G., and Scorcelli R. B. 2015. Kinetics of tetrataenite disordering. *Journal of Magnetism and Magnetic Materials* 375: 234–241. doi: 10.1016/j.jmmm.2014.09.051.

Doyle P. M., Nagashima K., Jogo K., and Krot A. N. 2013. ^{53}Mn-^{63}Cr chronometry reveals secondary fayalite in Asuka 881317 (CV3) and MacAlpine Hills (CO/CM-like) formed 4-5 Ma after CV CAIs (abstract #1793). 44th Lunar and Planetary Science Conference. CD-ROM.

Doyle P. M., Krot A. N., Nagashima K., Dobrica E., and Brearley A. J. 2014. Manganese-chromium ages of aqueous alteration of unequilibrated ordinary chondrites (abstract #1726). 45th Lunar and Planetary Science Conference. CD-ROM.

Eberhardt P., Eugster O., Geiss J., and Marti K. 1966. Rare gas measurements in 30 stone meteorites. *Zeitschrift für Naturforschung* 21a:414–426.

Eugster O. 1988. Cosmic ray production rates for ^{3}He, ^{21}Ne, ^{38}Ar, ^{83}Kr, and ^{126}Xe in chondrites based on ^{81}Kr-Kr exposure ages. *Geochimica et Cosmochimica Acta* 52:1649–1662.

Evans J. C., Reeves J. H., Rancitelli L. A., and Bogard D. D. 1982. Cosmogenic nuclides in recently fallen meteorites—Evidence for galactic cosmic ray variations during the period 1967–1978. *Journal of Geophysical Research* 87:5577–5587.

Friedrich J. M., Weisberg M. K., Ebel D. S., Biltz A. E., Corbett B. M., Iotzov I. V., Khan W. S., and Wolman M. D. 2015. Chondrule size and related physical properties: A compilation and evaluation of current data across all meteorite groups. *Chemie der Erde/Geochemistry*, doi:10.1016/j.chemer.2014.08.003.

Gattacceca J. and Rochette P. 2004. Toward a robust normalized magnetic paleointensity method applied to meteorites. *Earth and Planetary Science Letters* 227:377–393.

Gattacceca J., Rochette P., and Denise M. 2003. Magnetic properties of a freshly fallen LL ordinary chondrite: The Bensour meteorite. *Physics of the Earth and Planetary Interiors* 140:343–358.

Gattacceca J., Rochette P., Lagroix F., Mathe P.-E., and Zanda B. 2011. Low temperature magnetic transition of chromite in ordinary chondrites. *Geophysical Research Letters* 38:L10203. doi:10.1029/2011GL047173.

Gattacceca J., Suavet C., Rochette P., Weiss B. P., Winklhofer M., Uehara M., and Friedrich J. 2014. Metal phases in ordinary chondrites: Magnetic hysteresis

properties and implications for thermal history. *Meteoritics & Planetary Science* 49:652–676. doi:10.1111/maps.12268.

Graf T. and Marti K. 1994. Collisional records in LL-chondrites. *Meteoritics* 29:643–648.

Grossman J. N. and Brearley A. J. 2005. The onset of metamorphism in ordinary and carbonaceous chondrites. *Meteoritics & Planetary Science* 40:87–122.

Grossman J. N., Rubin A. E., Nagahara H., and King E. A. 1988. Properties of chondrules. In *Meteorites and the early solar system*, edited by Kerridge J. F. and Matthews M. S. Tucson, Arizona: The University of Arizona Press. pp. 619–659.

Guimon R. K., Weeks K. S., Keck B. D., and Sears D. W. G. 1984. Thermoluminescence as a palaeothermometer. *Nature* 311:363–365.

Guimon R. K., Keck B. D., and Sears D. W. G. 1985. Chemical and physical studies of type 3 chondrites—IV: Annealing studies of a type 3.4 ordinary chondrite and the metamorphic history of meteorites. *Geochimica et Cosmochimica Acta* 19:1515–1524.

Huss G. R., Rubin A. E., and Grossman J. N. 2006. Thermal metamorphism in chondrites. In *Meteorites and the early solar system II*, edited by Lauretta D. S. and McSween H. Y. Tucson, Arizona: The University of Arizona Press. pp. 567–586.

Jarosewich E. 1990. Chemical analyses of meteorites: A compilation of stony and iron metorite analyses. *Meteoritics* 25:323–337.

Jarosewich E. and Dodd R. T. 1981. Chemical variations among L-group chondrites, II. Chemical distinctions between L3 and LL3 chondrites. *Meteoritics* 16:83–91.

Jenniskens P., Rubin A. E., Yin Q.-Z., Sears D. W. G., Sandford S. A., Zolensky M. E., Krot A. N., Blair L., Kane D., Utas J., Verish R., Friedrich J. M., Wimpenny J., Eppich G. R., Ziegler K., Verosub K. L., Rowland D. J., Albers J., Gural P. S., Grigsby B., Fries M. D., Matson R., Johnston M., Silber E., Brown P, Yamakawa A., Sanborn M. E., Laubenstein M., Welten K. C., Nishiizumi K, Meier M. M. M., Busemann H., Clay P., Caffee M. W., Schmitt-Kopplin P., Hertkorn N., Glavin D. P., Callahan M. P., Dworkin J. P., Wu Q., Zare R. N., Grady M., Verchovsky S., Emel'Yanenko V., Naroenkov S., Clark D. L., Girten B., and Worden P. S. 2014. Fall, recovery, and characterization of the Novato L6 chondrite breccia. *Meteoritics & Planetary Science* 49:1388–1425.

Kallemeyn G. W., Rubin A. E., Wang D., and Wasson J. T. 1989. Ordinary chondrites: Bulk compositions, classification, lithophile-element fractionations, and composition-petrographic type relationships. *Geochimica et Cosmochimica Acta* 53:2747–2767.

Kita N. T., Welten K. C., Valley J. W., Spicuzza M. J., Nakashima D., Tenner T. J., Ushikubo T., MacPherson G. J., Welzenbach L., Heck P. R., Davis A. M., Meier M. M. M., Wieler R., Caffee M. W., Laubenstein M., and Nishiizumi K. 2013. Fall, classification, and exposure history of the Mifflin L5 chondrite. *Meteoritics and Planetary Science* 48:641–655.

Krot A. N. and Nagashima K. 2012. Oxygen-isotope systematics of the fayalite-bearing assemblages in MAC 88107, CO-like carbonaceous chondrite (abstract #5338). *Meteoritics & Planetary Science* 47:A231.

Krot A. N., Keil K., Goodrich C. A., Scott E. R. D., and Weisberg M. K. 2014. Classification of meteorites and their genetic relationships. In *Meteorites and cosmochemical processes*, 2nd ed., edited by Davis A. M., Holland H. D., and Turekian K. K. Treatise on geochemistry, vol. 1. Amsterdam: Elsevier. pp. 1–63.

Leya I. and Masarik J. 2009. Cosmogenic nuclides in stony meteorites revisited. *Meteoritics & Planetary Science* 44:1061–1086.

Lodders K. and Fegley B. Jr. 1998. *The planetary scientist's companion*. New York: Oxford University Press. p. 371.

McKie D. and McConnell J. D. C. 1963. The kinetics of the low-high transformation in albite. I. Amelia albite under dry conditions. *Mineralogical Magazine* 33: 581–588.

McSween H. Y. Jr. and Huss G. R. 2010. *Cosmochemistry*. Cambridge, UK: Cambridge University Press. p. 549.

Miller M. F., Franchi I. A., Sexton A. S., and Pillinger C. T. 1999. High precision $\delta^{17}O$ isotope measurements of oxygen from silicates and other oxides: Method and applications. *Rapid Communication in Mass Spectrometry* 13:1211–1217.

Moutinho A. and Zucolotto E. 2014. The 2013 Vicência meteorite—Field report. *Meteorite* 20:27–32.

Nelson V. E. and Rubin A. E. 2002. Size-frequency distributions of chondrules and chondrule fragments in LL3 chondrites: Implications for parent body fragmentation of chondrules. *Meteoritics & Planetary Science* 37:1361–1376.

Nishiizumi K., Regnier S., and Marti K. 1980. Cosmic ray exposure ages of chondrites, pre-irradiation and constancy of cosmic ray flux in the past. *Earth and Planetary Science Letters* 56:156–170.

Nishiizumi K., Caffee M. W., Hamajima Y., Reedy R. C., and Welten K. C. 2014. Exposure history of the Sutter's Mill carbonaceous chondrite. *Meteoritics & Planetary Science* 49:2056–2063. doi:10.1111/maps.12297.

Ott U. 2014. Planetary and pre-solar noble gases in meteorites. *Chemie der Erde/Geochemistry* 74:519–550. doi:10.1016/j.chemer.2014.01.003.

Popova O. P., Jenniskens P., Emel'yanenko V., Kartashova A., Biryukov E., Khaibrakhmanov S., Shuvalov V., Rybnov Y., Dudorov A., Grokhovsky V. I., Badyukov D. D., Yin Q.-Z., Gural P. S., Albers J., Granvik M., Evers L. G., Kuiper J., Kharlamov V., Solovyov A., Rusakov Y. S., Korotkiy S., Serdyuk I., Korochantsev A. V., Larionov M. Y., Glazachev D., Mayer A. E., Gisler G., Gladkovsky S. V., Wimpenny J., Sanborn M. E., Yamakawa A., Verosub K., Rowland D. J., Roeske S., Botto N. W., Friedrich J. M., Zolensky M., Le L., Ross D., Ziegler K., Nakamura T., Ahn I., Lee J. I., Zhou Q., Li X.-H., Li Q.-L., Liu Y., Tang G.-Q., Hiroi T., Sears D., Weinstein I. A., Vokhmintsev A. S., Ishchenko A. V., Schmitt-Kopplin P., Hertkorn N., Nagao K., Haba M. K., Komatsu M., and Mikouchi T. (the Chelyabinsk Airburst Consortium). 2013. Chelyabinsk airburst, damage assessment, meteorite recovery, and characterization. *Science* 342:1069–1073.

Quirico E., Raynal P.-I., and Bourot-Denise M. 2003. Metamorphic grade of organic matter in six unequilibrated ordinary chondrites. *Meteoritics & Planetary Science* 38:795–811.

Rambaldi E. R. and Wasson J. T. 1984. Metal and associated phases in Krymka and Chainpur: Nebular formational processes. *Geochimica et Cosmochimica Acta* 48:1885–1897.

Rancourt D. G. and Scorzelli R. B. 1995. Low-spin γ-Fe-Ni (γLS) proposed as a new mineral in Fe-Ni-bearing meteorites: Epitaxial intergrowth of γLS and tetrataenite as a possible equilibrium state at ~ 20–40 at% Ni. *Journal of Magnetism and Magnetic Materials* 150:30–36.

Rochette P., Sagnotti L., Bourot-Denise M., Consolmagno G., Folco L., Gattacceca J., Osete M. L., and Pesonen L. 2003. Magnetic classification of stony meteorites: 1. Ordinary chondrites. *Meteoritics & Planetary Science* 38:251–258.

Rubin A. E. 1990. Kamacite and olivine in ordinary chondrites: Intergroup and intragroup relationships. *Geochimica et Cosmochimica Acta* 54:1217–1232.

Scherer P., Herrmann S., and Schultz L. 1998. Noble gases in twenty-one Saharan LL-chondrites: Exposure ages and possible pairings. *Meteoritics & Planetary Science* 33:259–265.

Schmitt-Kopplin P., Harir M., Kanawati B., Tziotis D., Hertkorn N., and Gabelica Z. 2012. Chemical footprint of the solvent soluble extraterrestrial organic matter occluded in Soltmany ordinary chondrite. *Meteorites* 1–2:79–92.

Schultz L. and Franke L. 2004. *Helium, neon, and argon in meteorites—A data collection*. Mainz: Max-Planck-Institut für Chemie. CD-ROM.

Schultz L., Weber H. W., and Begemann F. 1991. Noble gases in H-chondrites and potential differences between Antarctic and non-Antarctic meteorites. *Geochimica et Cosmochimica Acta* 55:59–66.

Sears D. W. G., Grossman J. N., Melcher C. L., Ross L. M., and Mills A. A. 1980. Measuring the metamorphic history of unequilibrated ordinary chondrites. *Nature* 287:791–795.

Sears D. W. G., Lu J., Benoit P. H., DeHart J. M., and Lofgren G. E. 1992. A compositional classification scheme for meteoritic chondrules. *Nature* 357:207–210.

Sears D. W. G., Huang S., and Benoit P. H. 1995. Chondrule formation, metamorphism, brecciation, an important new primary chondrule group, and the classification of chondrules. *Earth and Planetary Science Letters* 131:27–39.

Sears D. W. G., Ninagawa K., and Singhvi A. K. 2013. Luminescence studies of extraterrestrial materials: Insights into their recent radiation and thermal histories and into their metamorphic history. *Chemie der Erde—Geochemistry* 73:1–37.

Spergel M. S., Reedy R. C., Lazareth O. W., Levy P. W., and Slatest L. A. 1986. Cosmogenic neutron-capture-produced nucleides in stony meteorites. *16th Proceedings of the Lunar & Planetary Science Conference, Journal of Geophysical Research Supplement* 91:D483–D494.

Stöffler D., Keil K., and Scott E. R. D. 1991. Shock metamorphism of ordinary chondrites. *Geochimica et Cosmochimica Acta* 55:3845–3867.

Uehara M., Gattacceca J., Leroux H., Jacob D., and van der Beek C. J. 2011. Magnetic microstructures of metal grains in equilibrated ordinary chondrites and implications for paleomagnetism of meteorites. *Earth and Planetary Science Letters* 306:241–252.

Wasson J. T. and Kallemeyn G. W. 1988. Compositions of chondrites. *Philosophical Transactions of the Royal Society of London* A325:535–544.

Wood J. A. 1967. Olivine and pyroxene compositions in type II carbonaceous chondrites. *Geochimica et Cosmochimica Acta* 31:2095–2108.

SUPPORTING INFORMATION

Additional supporting information may be found in the online version of this article:

Data S1: Analytical techniques.

Fig S1: The Vicência meteorite, before samples were taken for scientific study, with a 1 cm^3 scale.

Fig S2a: The village Borracha near the small city of Vicência, where the Vicência meteorite fell, and where Mr. Adeildo Silva lives.

Fig S2b: Abundant banana plantations around the village of Borracha near Vicência.

Fig S3a: The impact pit with the Vicência meteorite in the village of Borracha near Vicência.

Fig S3b: Mr. Adeildo Silva holding the Vicência meteorite in the impact pit.

Fig S4: From left to right: Andre Moutinho and Maria E. Zucolotto upon arrival at Borracha, with Mr. Adeildo Silva.

Fig S5: Slightly enlarged image of Fig. 1 of the cut surface of the Vicência chondrite, showing abundant and beautifully developed chondrules and what appear to be chondrule, mineral, and rock fragments, embedded into a gray to black, fine-grained matrix.

Fig S6: Photomicrographs of the texture of Vicência in a) transmitted, plane polarized light; b) transmitted light, crossed polars; and c) reflected light, showing well-developed radial pyroxene and porphyritic chondrules. In c), white is metallic Fe, Ni, and tan is troilite.

Fig S7: Metallographic cooling rates of taenite grains at 500–600 °C in Vicência, indicating that Vicência cooled at ~50–60 K Ma^{-1}. The revised cooling rate curves are from Willis and Goldstein (1981).

Fig S8: Baseline-corrected Raman spectra from the matrix of Vicência (black), QUE97008 (gray), and GRO95544 (white), showing the first-order carbon D- and G-bands. The D-band (~1350 cm^{-1}) is from disordered graphite and the G-band (~1600 cm^{-1}) is from structured graphite. The width of the D-band (FWHM-D) and the ratio of the intensities of the D- and G-bands (I_D/I_G) are sensitive to thermal metamorphism (Quirico et al. 2003; Bonal et al. 2006, 2007).

Fig S9: Abundance ratio diagram showing H-group ordinary chondrite and Cr-normalized lithophile element data for CI, L, and LL chondrites (Wasson and Kallemeyn 1988; Kallemeyn et al. 1989) together with Vicência as triangles. The refractory lithophile data (Sc although Lu) confirm that Vicência is an ordinary chondrite.

Fig S10: Thermal evolution of Zero Field Cooled Low-Temperature sIRM (ZFC LT-sIRM) between 10 and 300 K for Semarkona (LL3.0), Krymka (LL3.1), Mezö-Madaras (LL3.7), Bensour (LL6), and Vicência (452 mg sample). The Verwey and chromite transition temperatures are indicted. Modified from Gattacceca

et al. (2011) and reprinted with permission from Geophysical Research Letters.

Fig S11: a) ICR-FT/MS mass spectrum in ESI(-) of the methanol extract of Vicência meteorite showing 60.000 signals in the mass range converted into 9500 formula and filtered to 1845 validated CHNOS compositions; b) detail on nominal mass 319 with some assignment examples of CHO and CHOS elementary compositions for Vicência compared to LL5 Chelyabinsk and LL6 Kilabo showing a loss in signature from LL3.2 to LL6.

Fig S12: van Krevelen representation of the three meteorites in the H/C versus O/C and H/C versus m/z domains. The bubble intensity corresponds to the intensity of the corresponding signals in the mass spectra and the color code is given as follow: blue CHO, green CHOS, orange CHNO, and red CHNOS species. The number in the circle correspond to the total amount of elementary compositions calculated for the particular samples and the color the relative abundance of the various species.